Bedrock controls on water and energy partitioning across the western contiguous United States

Robert Ehlert[1], W. Jesse Hahm[1], David N Dralle[2], Daniella Rempe[3], and Diana M. Allen[1]

[1]Simon Fraser University
[2]Pacific Southwest Research Station, United States Forest Service
[3]University of Texas at Austinn

November 22, 2023

Abstract

Across diverse biomes and climate types, plants use water stored in bedrock to sustain transpiration. Bedrock water storage ($S_{bedrock}$, mm), in addition to soil moisture, thus plays an important role in water cycling and should be accounted for in the context of surface energy balances and streamflow generation. Yet, the extent to which bedrock water storage impacts hydrologic partitioning and influences latent heat fluxes has yet to be quantified at large scales. This is particularly important in Mediterranean climates, where the majority of precipitation is offset from energy delivery and plants must rely on water retained from the wet season to support summer growth. Here we present a simple water balance approach and random forest model to quantify the role of $S_{bedrock}$ on controlling hydrologic partitioning and land surface energy budgets. Specifically, we track evapotranspiration in excess of precipitation and mapped soil water storage capacity (S_{soil}, mm) across the western US in the context of Budyko's water partitioning framework. Our findings indicate that $S_{bedrock}$ is necessary to sustain plant growth in forests in the Sierra Nevada — some of the most productive forests on Earth — as early as April every year, which is counter to the current conventional thought that bedrock is exclusively used late in the dry season under extremely dry conditions. We show that the average latent heat flux used in evapotranspiration of $S_{bedrock}$ can exceed 100 W/m^{2} during the dry season and the proportion of water that returns to the atmosphere would decrease dramatically without access to $S_{bedrock}$.

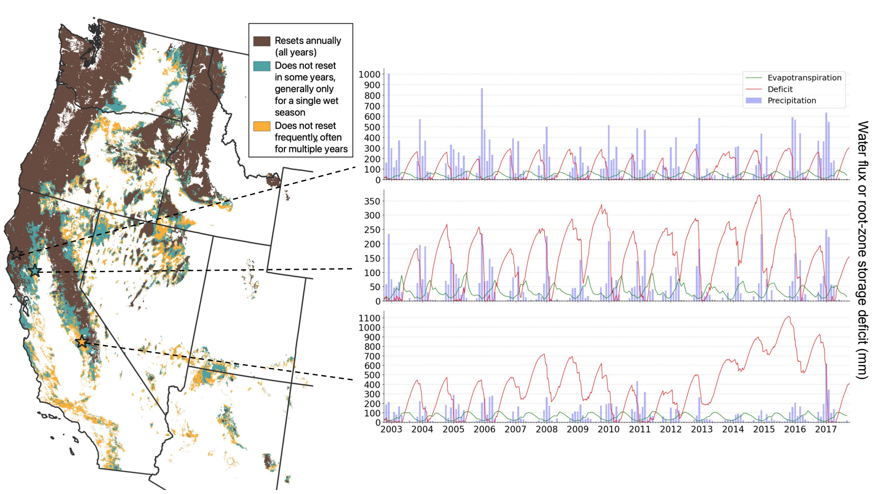

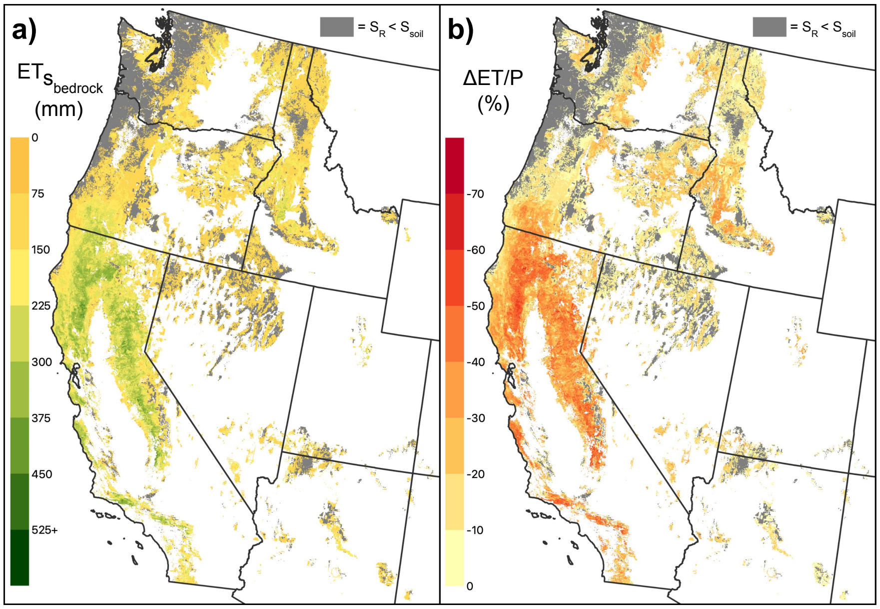
a)
= S_R < S_{soil}
$ET_{s_{bedrock}}$ (mm)
0
75
150
225
300
375
450
525+
b)
= S_R < S_{soil}
ΔET/P (%)
-70
-60
-50
-40
-30
-20
-10
0

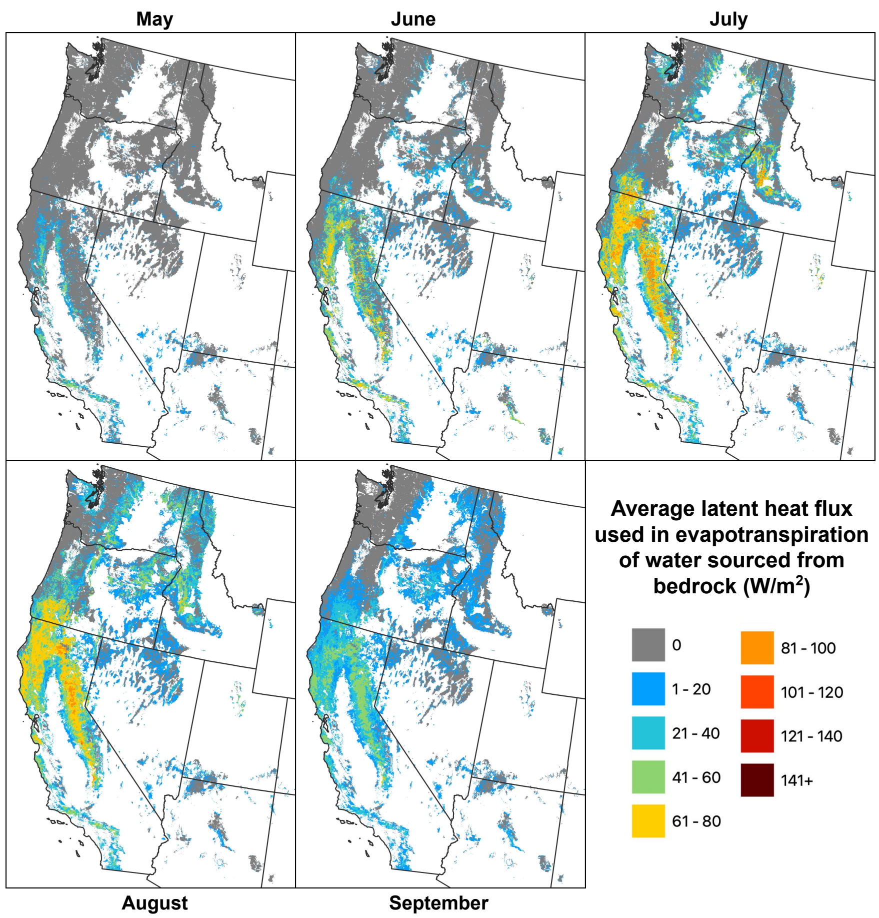
May
June
July
August
September
Average latent heat flux used in evapotranspiration of water sourced from bedrock (W/m^2)
0
1 - 20
21 - 40
41 - 60
61 - 80
81 - 100
101 - 120
121 - 140
141+

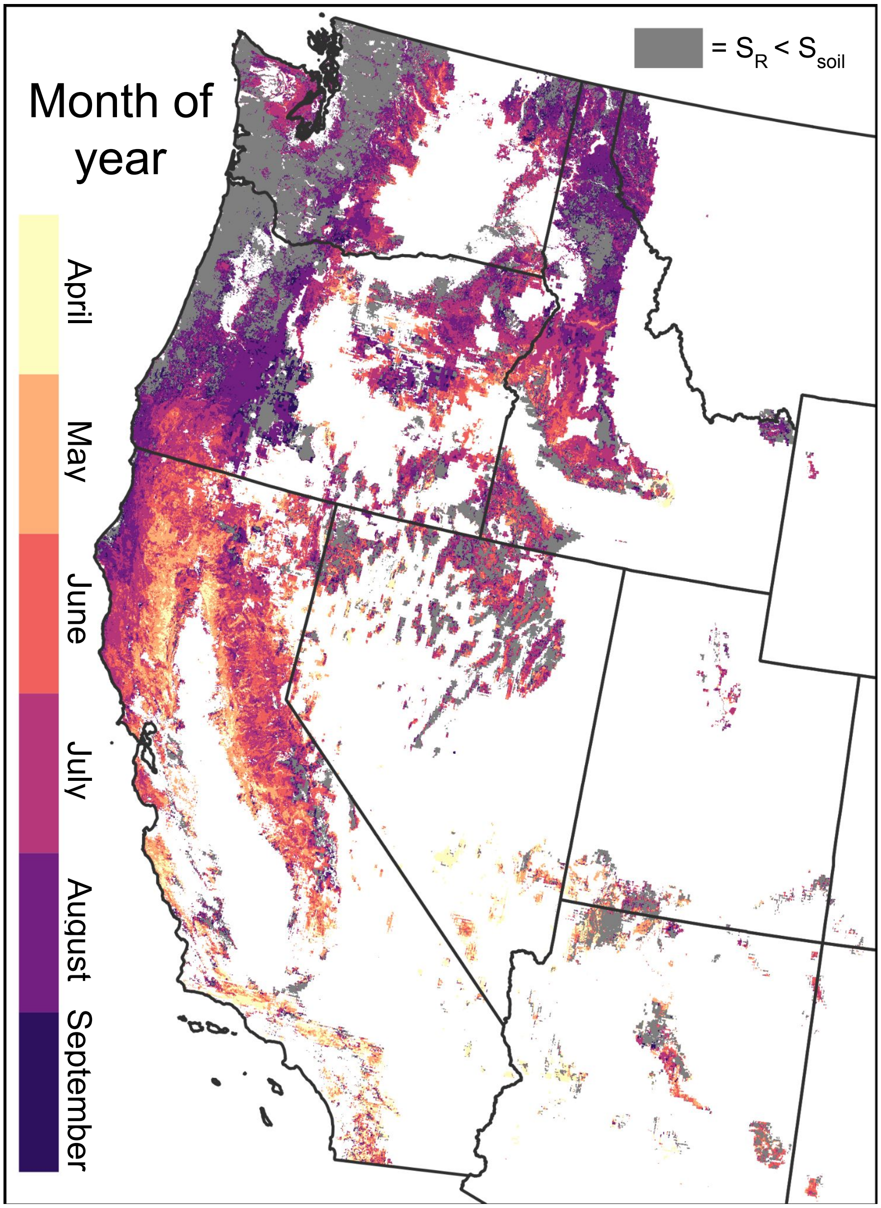

= $S_R < S_{soil}$
Month of year
April
May
June
July
August
September

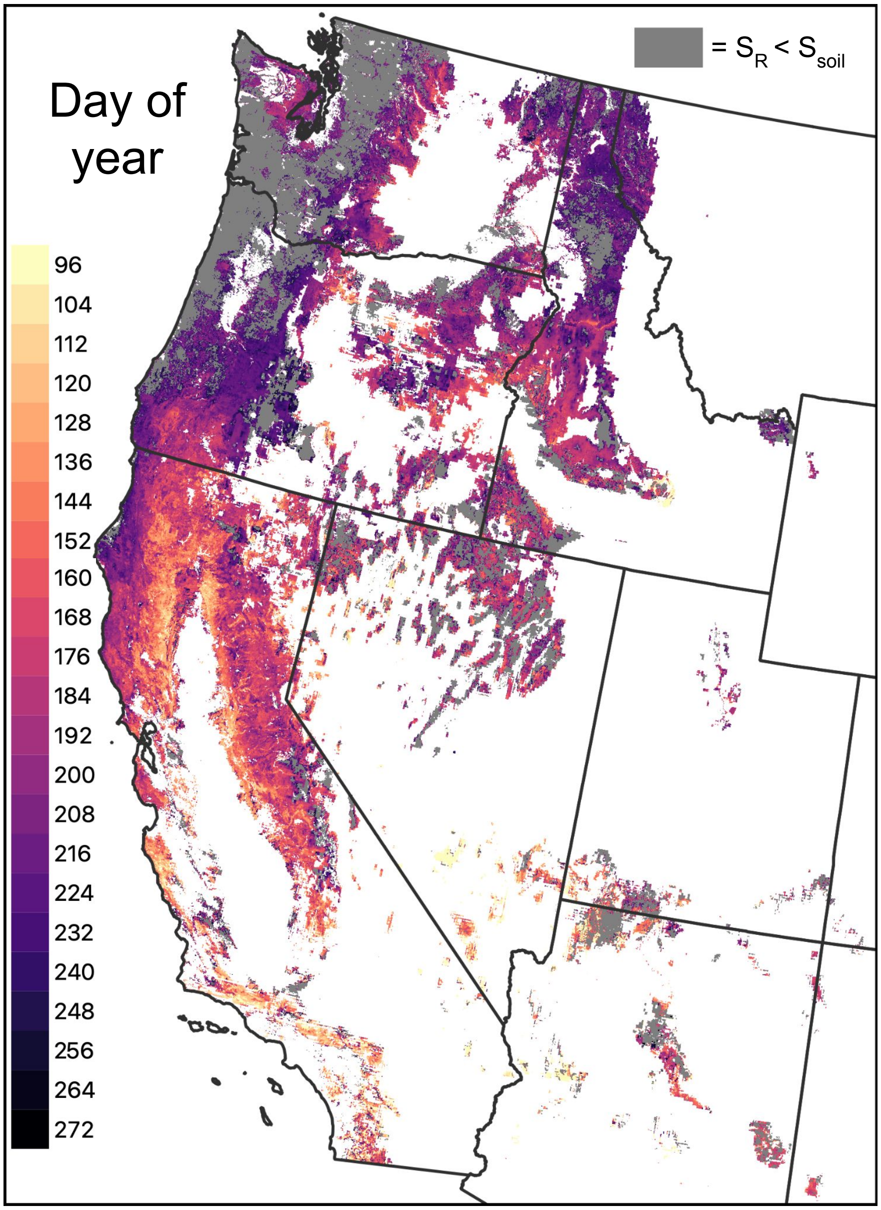

Day of year
= $S_R < S_{soil}$
96
104
112
120
128
136
144
152
160
168
176
184
192
200
208
216
224
232
240
248
256
264
272

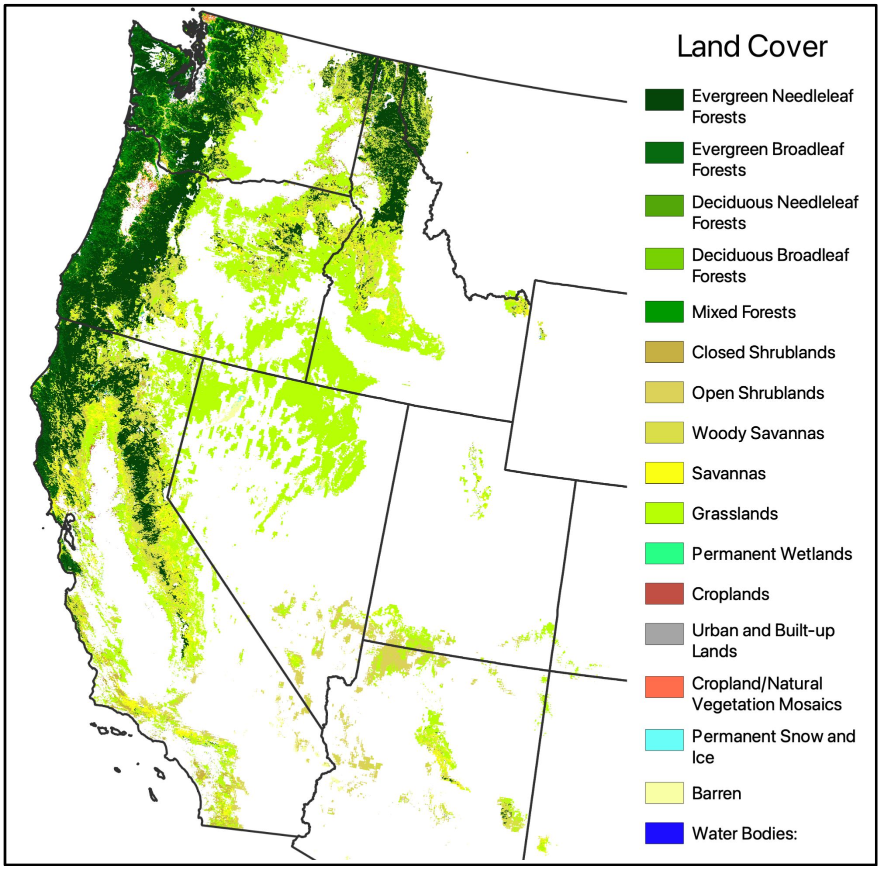

Land Cover
Evergreen Needleleaf Forests
Evergreen Broadleaf Forests
Deciduous Needleleaf Forests
Deciduous Broadleaf Forests
Mixed Forests
Closed Shrublands
Open Shrublands
Woody Savannas
Savannas
Grasslands
Permanent Wetlands
Croplands
Urban and Built-up Lands
Cropland/Natural Vegetation Mosaics
Permanent Snow and Ice
Barren
Water Bodies:

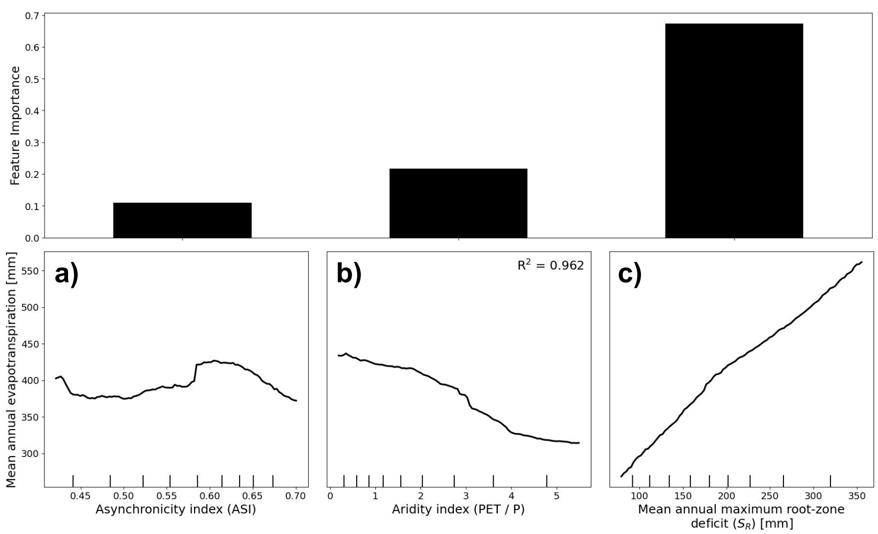

Feature Importance
Mean annual evapotranspiration [mm]
a)
b)
c)
R^2 = 0.962
Asynchronicity index (ASI)
Aridity index (PET / P)
Mean annual maximum root-zone deficit (S_R) [mm]

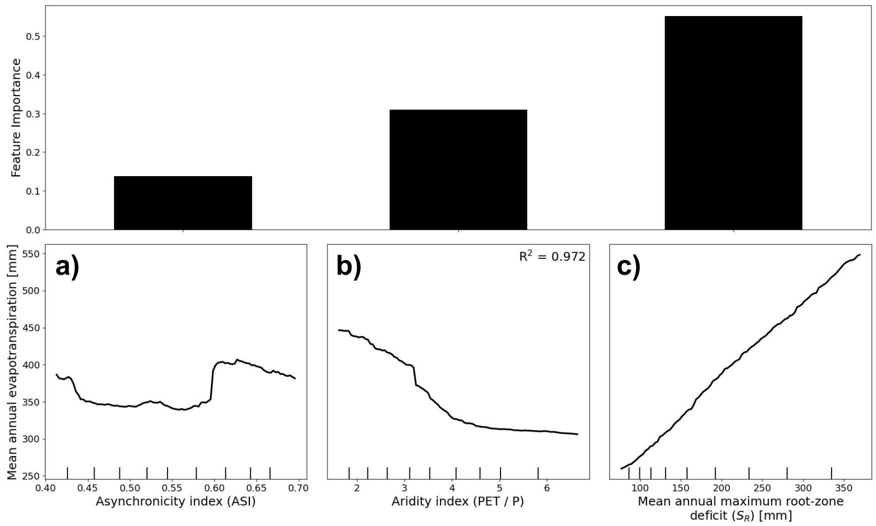
Feature Importance
a)
b)
R^2 = 0.972
c)
Mean annual evapotranspiration [mm]
Asynchronicity index (ASI)
Aridity index (PET / P)
Mean annual maximum root-zone deficit (S_R) [mm]

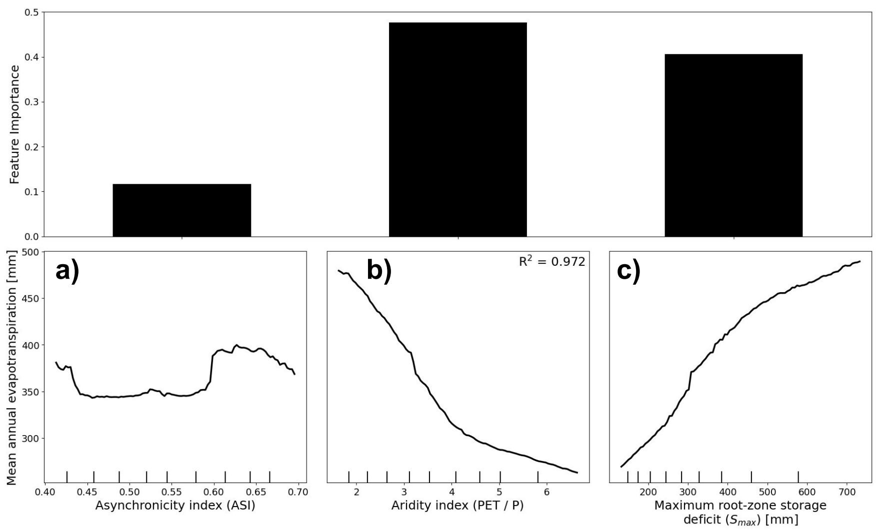
Feature Importance
a)
b)
R^2 = 0.972
c)
Mean annual evapotranspiration [mm]
Asynchronicity index (ASI)
Aridity index (PET / P)
Maximum root-zone storage deficit (S_{max}) [mm]

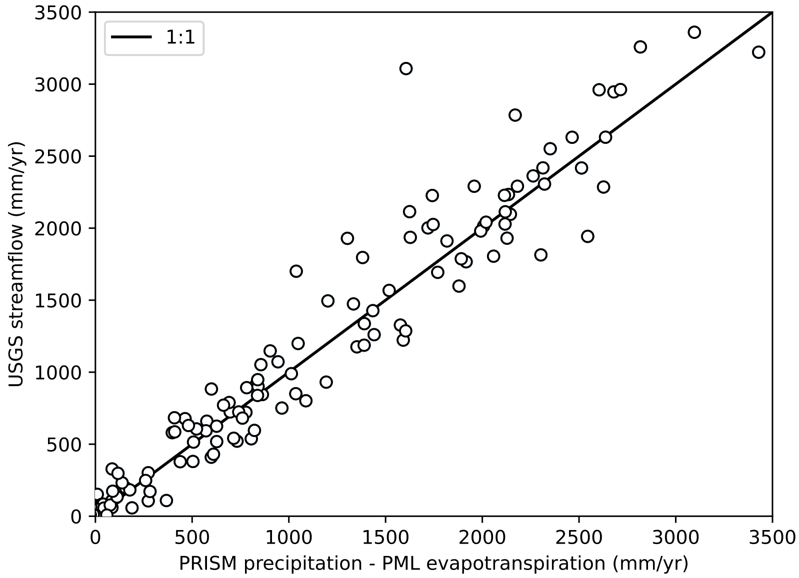
1:1
USGS streamflow (mm/yr)
PRISM precipitation - PML evapotranspiration (mm/yr)
0
500
1000
1500
2000
2500
3000
3500

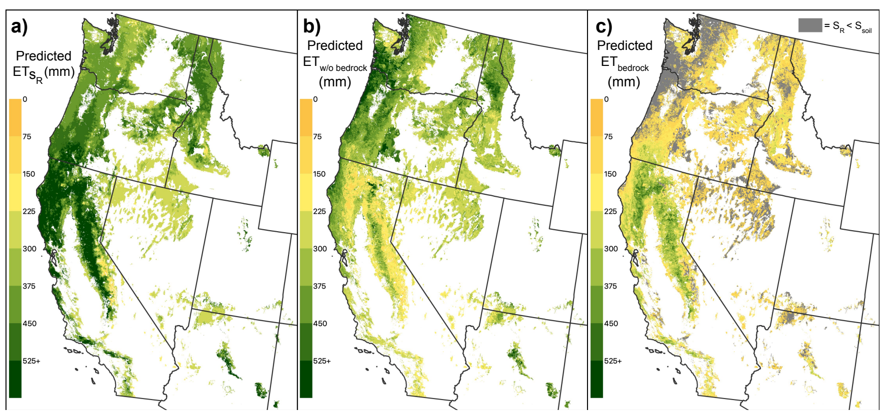
a)
Predicted ET_{S_R} (mm)
b)
Predicted $ET_{w/o\ bedrock}$ (mm)
c)
Predicted $ET_{bedrock}$ (mm)
= $S_R < S_{soil}$
0
75
150
225
300
375
450
525+

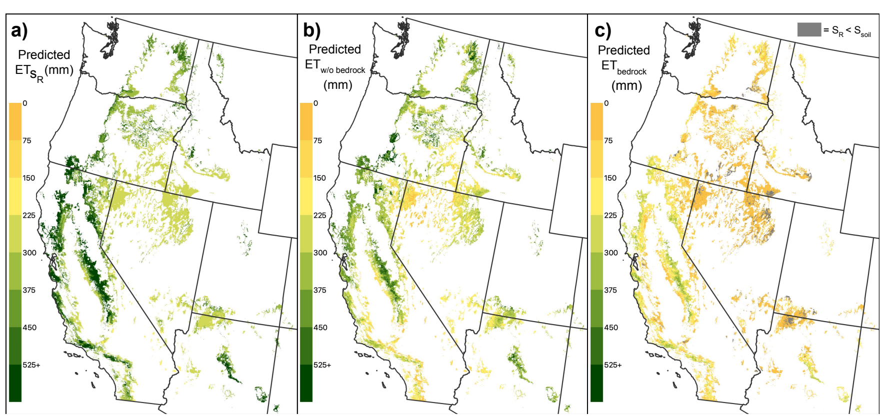
a)
Predicted ET_{S_R} (mm)
b)
Predicted $ET_{w/o\ bedrock}$ (mm)
c)
Predicted $ET_{bedrock}$ (mm)
= $S_R < S_{soil}$
0
75
150
225
300
375
450
525+

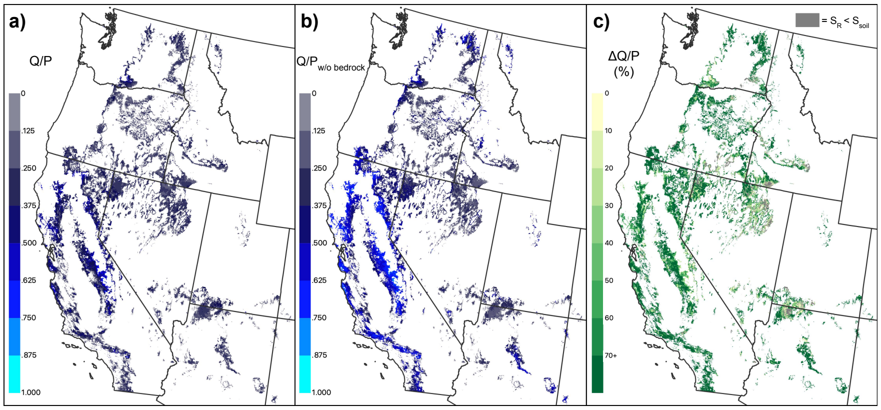
a)
Q/P
0
.125
.250
.375
.500
.625
.750
.875
1.000
b)
Q/P w/o bedrock
0
.125
.250
.375
.500
.625
.750
.875
1.000
c)
= S_R < S_soil
ΔQ/P
(%)
0
10
20
30
40
50
60
70+

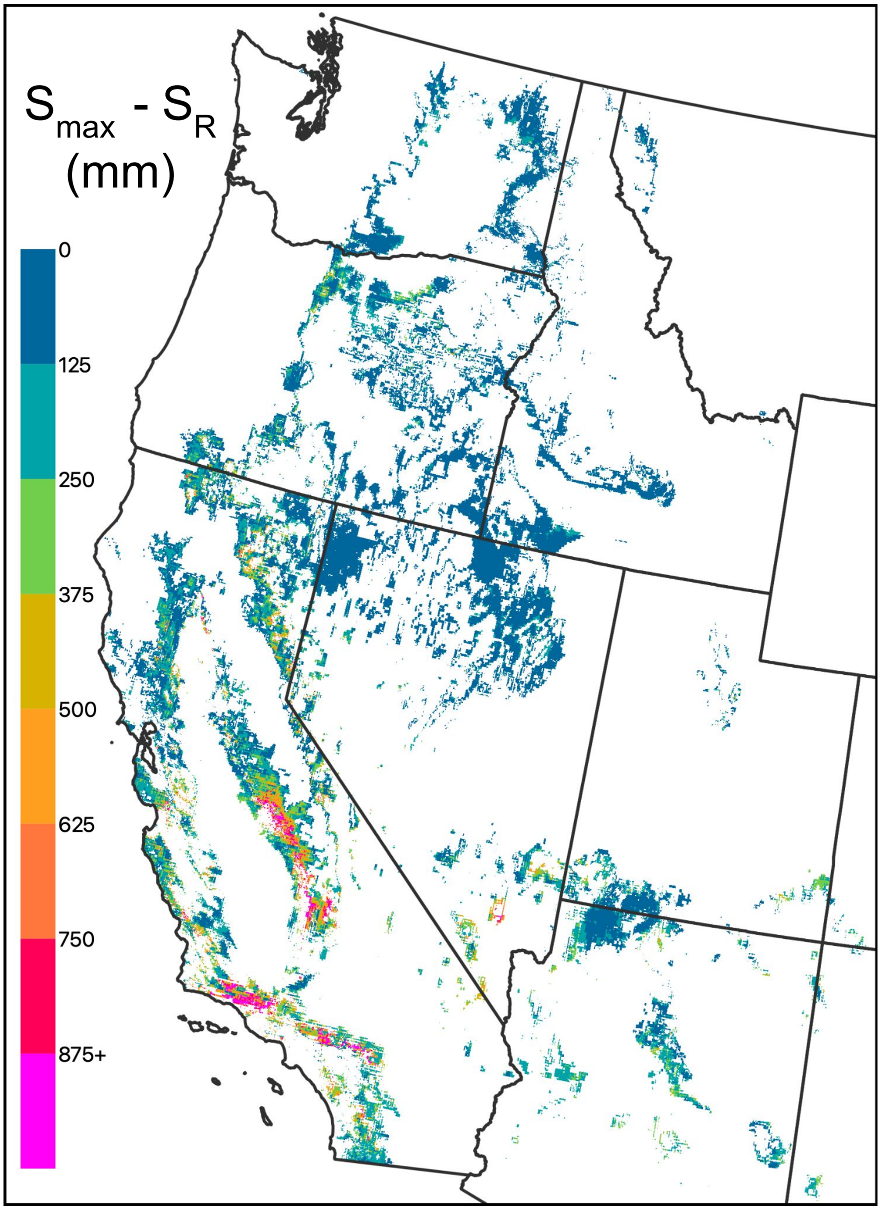
$S_{max} - S_R$ (mm)
0
125
250
375
500
625
750
875+

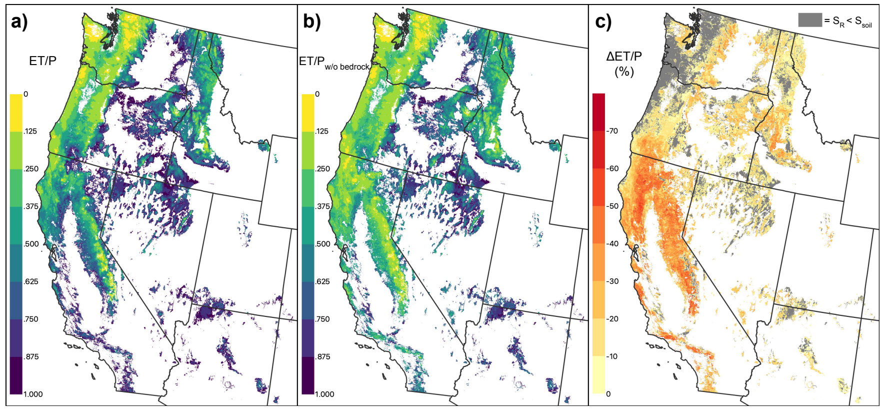
a)
ET/P
b)
ET/P$_{w/o\ bedrock}$
c)
= $S_R < S_{soil}$
ΔET/P
(%)

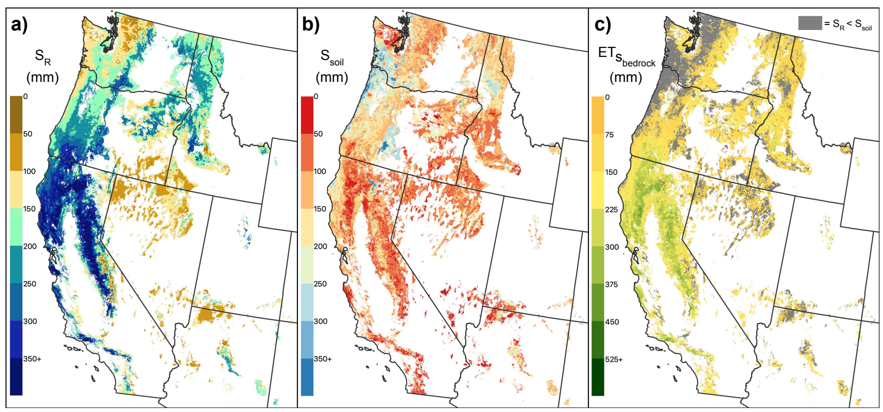
a)
S_R
(mm)
b)
S_{soil}
(mm)
c)
= $S_R < S_{soil}$
$ET_{S_{bedrock}}$
(mm)

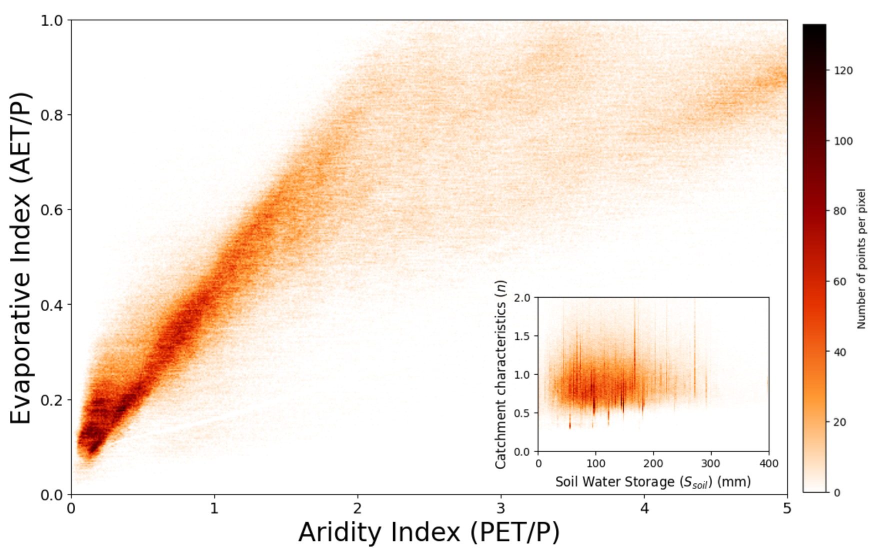
Evaporative Index (AET/P)
Aridity Index (PET/P)
Number of points per pixel
Catchment characteristics (n)
Soil Water Storage (S_{soil}) (mm)

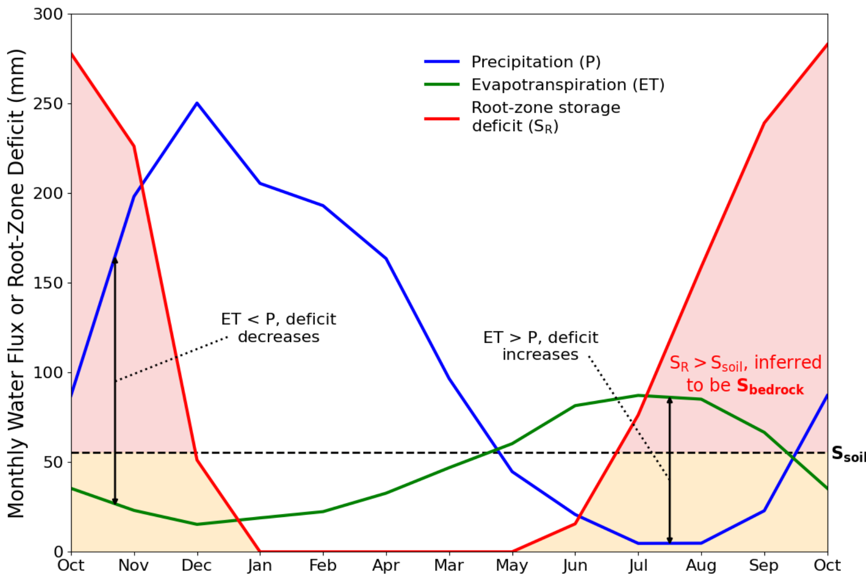
Precipitation (P)
Evapotranspiration (ET)
Root-zone storage deficit (S_R)
Monthly Water Flux or Root-Zone Deficit (mm)
ET < P, deficit decreases
ET > P, deficit increases
$S_R > S_{soil}$, inferred to be $\mathbf{S_{bedrock}}$
$\mathbf{S_{soil}}$
Oct
Nov
Dec
Jan
Feb
Apr
Mar
May
Jun
Jul
Aug
Sep
Oct

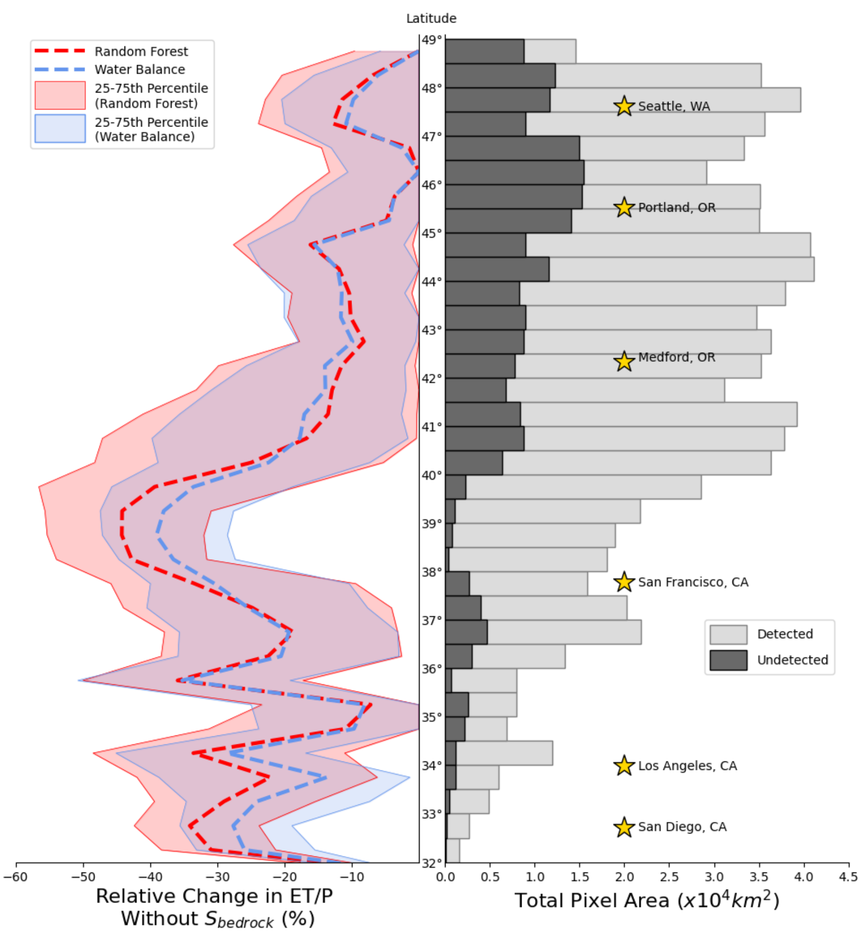
Random Forest
Water Balance
25-75th Percentile (Random Forest)
25-75th Percentile (Water Balance)
Latitude
Seattle, WA
Portland, OR
Medford, OR
San Francisco, CA
Los Angeles, CA
San Diego, CA
Detected
Undetected
Relative Change in ET/P Without $S_{bedrock}$ (%)
Total Pixel Area ($x10^4 km^2$)

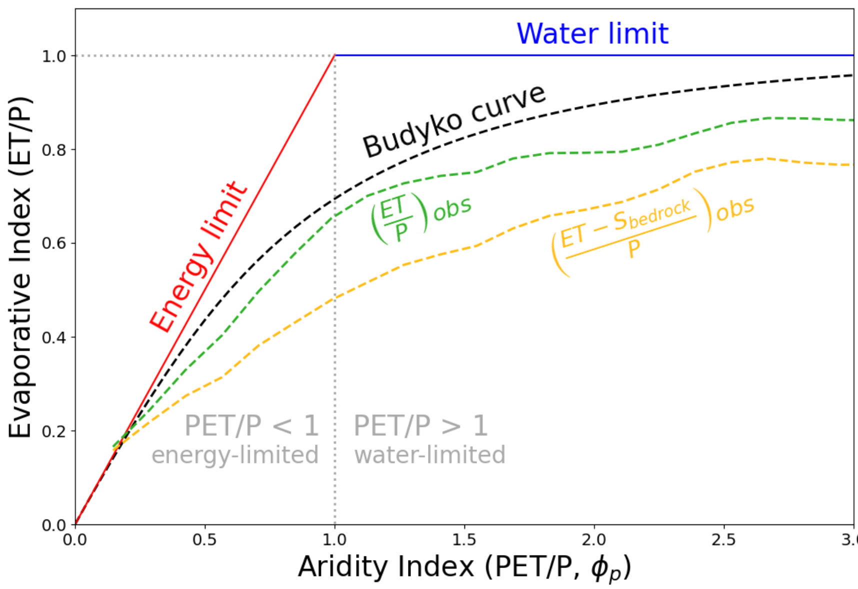

Water limit
Budyko curve
Energy limit
$\left(\frac{ET}{P}\right)obs$
$\left(\frac{ET - S_{bedrock}}{P}\right)obs$
PET/P < 1
energy-limited
PET/P > 1
water-limited
Evaporative Index (ET/P)
Aridity Index (PET/P, ϕ_p)
0.0
0.2
0.4
0.6
0.8
1.0
0.0
0.5
1.0
1.5
2.0
2.5
3.0

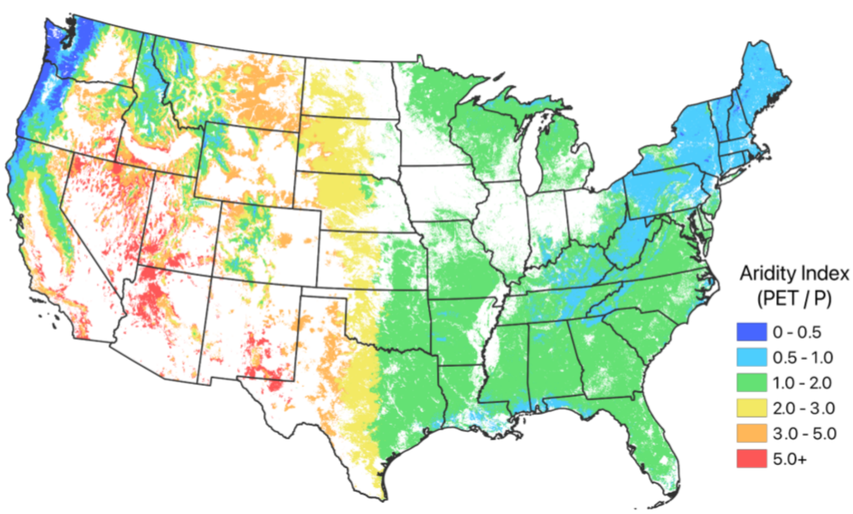

Aridity Index
(PET / P)
0 - 0.5
0.5 - 1.0
1.0 - 2.0
2.0 - 3.0
3.0 - 5.0
5.0+

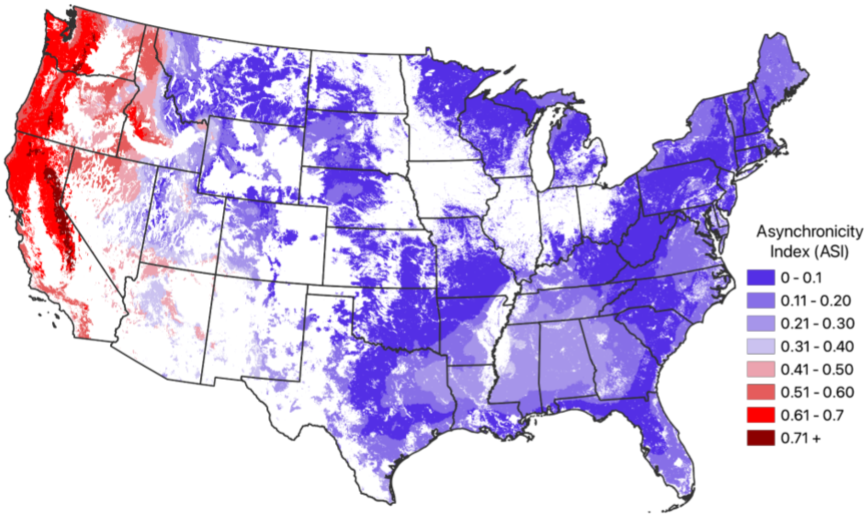
Asynchronicity Index (ASI)
0 - 0.1
0.11 - 0.20
0.21 - 0.30
0.31 - 0.40
0.41 - 0.50
0.51 - 0.60
0.61 - 0.7
0.71 +

Bedrock controls on water and energy partitioning across the western contiguous United States

Robert S. Ehlert[1], W. Jesse Hahm[1], David N. Dralle[2], Daniella M. Rempe[3], Diana M. Allen[4]

[1]Department of Geography, Simon Fraser University, Burnaby, BC, Canada
[2]Pacific Southwest Research Station, United States Forest Service, Davis, CA, USA
[3]Department of Geological Sciences, Jackson School of Geosciences, University of Texas at Austin, Austin, TX, USA
[4]Department of Earth Sciences, Simon Fraser University, Burnaby, BC, Canada

Key Points:

- Plant use of bedrock storage impacts water partitioning in the seasonally dry, western contiguous United States
- Dry season latent heat flux due to bedrock-sourced evapotranspiration could moderate summer high temperatures
- Plants may exhaust soil water storage and require bedrock water as early as April each year

Corresponding author: Robert Ehlert, robert_ehlert@sfu.ca

Abstract

Across diverse biomes and climate types, plants use water stored in bedrock to sustain transpiration. Bedrock water storage ($S_{bedrock}$, mm), in addition to soil moisture, thus plays an important role in water cycling and should be accounted for in the context of surface energy balances and streamflow generation. Yet, the extent to which bedrock water storage impacts hydrologic partitioning and influences latent heat fluxes has yet to be quantified at large scales. This is particularly important in Mediterranean climates, where the majority of precipitation is offset from energy delivery and plants must rely on water retained from the wet season to support summer growth. Here we present a simple water balance approach and random forest model to quantify the role of $S_{bedrock}$ on controlling hydrologic partitioning and land surface energy budgets. Specifically, we track evapotranspiration in excess of precipitation and mapped soil water storage capacity (S_{soil}, mm) across the western US in the context of Budyko's water partitioning framework. Our findings indicate that $S_{bedrock}$ is necessary to sustain plant growth in forests in the Sierra Nevada — some of the most productive forests on Earth — as early as April every year, which is counter to the current conventional thought that bedrock is exclusively used late in the dry season under extremely dry conditions. We show that the average latent heat flux used in evapotranspiration of $S_{bedrock}$ can exceed 100 W/m^2 during the dry season and the proportion of water that returns to the atmosphere would decrease dramatically without access to $S_{bedrock}$.

Plain Language Summary

Plants frequently use water stored in bedrock ($S_{bedrock}$) in order to grow. However, the proportion of precipitation that returns to the atmosphere (evapotranspiration) vs. to streams (runoff) as well as how much latent heat — the energy associated with evaporating water — is used as a result of access to $S_{bedrock}$ has not been measured. In Mediterranean climates, such as the western US, the majority of energy (sunlight) is received during the dry season and plants must rely on water stored belowground during the wet season to sustain summer growth. In this study, we present two methods for calculating how much $S_{bedrock}$ influences the amount of water returning to the atmosphere vs. streams and what that corresponds to in terms of latent heat energy at the surface. We use gridded data to compare the amount of water entering (precipitation) and exiting (evapotranspiration) the area and use a mapped soil water storage capacity product to draw conclusions about the timing and magnitude of plant transpiration that is a result of access to bedrock water. Our findings indicate that some of the Earth's most productive forests use $S_{bedrock}$ early in the growing season, consuming over 100 W/m^2 of latent heat energy in the summer.

1 Introduction

Globally, a greater proportion of precipitation is returned to the atmosphere via evapotranspiration (ET) compared to oceans via streamflow (Q) (Jasechko et al., 2013; Trenberth et al., 2007). Locally, precipitation partitioning between streamflow and evapotranspiration is mediated by local climate (Budyko, 1974). In asynchronous climates, where the majority of precipitation is offset from energy delivery (Feng et al., 2019; Klos et al., 2018), a substantial proportion of plant transpiration is sourced from bedrock water storage ($S_{bedrock}$) (Hahm et al., 2020; Hubbert, Beyers, & Graham, 2001; McCormick et al., 2021; Rempe & Dietrich, 2018; Rose et al., 2003; Witty et al., 2003). Yet, there have been no attempts to quantify the extent to which bedrock water storage alters annual hydrologic partitioning in asynchronous climates. Moreover, global climate models (GCMs) typically only consider soil moisture dynamics when modelling latent heat flux — the transfer of heat between the terrestrial biosphere and atmosphere — which may work well for humid regions but poorly accounts for climates where plants rely on water stored deep in the subsurface to compensate for a lack of precipitation during the summer dry season. Soil moisture content has been shown to influence extreme daily temperatures (Durre et al., 2000), regulate the number of large fires (Jensen et al., 2018) and length of the wildfire season (Rakhmatulina et al., 2021), and was a contributing factor to the 2003 record-breaking heat wave in Europe (Fischer et al., 2007). It stands to reason that bedrock water storage, in addition to soil moisture, should be considered when evaluating land energy budgets and hydrologic partitioning.

The relative magnitudes of the water balance components at a location are dictated by the availability of water supply (precipitation) vs. demand (energy) (Budyko, 1974). Over long time frames, where change in storage (ΔS) can be considered negligible, the ratio of evapotranspiration relative to precipitation (i.e. the evaporative index, $\epsilon = ET/P = 1 - Q/P$) can be estimated based on the ratio of potential evapotranspiration (PET) relative to precipitation (the aridity index, $\Phi = PET/P$; see Table 1 for a list of variables and their definitions). In practice, most catchments fall near a single curve — the Budyko curve — when plotted in ET/P versus PET/P space, with deviations from this curve resulting from seasonality (Feng et al., 2012; Hickel & Zhang, 2006; Xing et al., 2018), vegetation cover (Chen et al., 2013; R. Donohue et al., 2007; M. Liu et al., 2022; L. Zhang et al., 2001), subsurface storage dynamics (Milly, 1994a), and other catchment-specific characteristics (e.g. Lhomme & Moussa, 2016; H. Yang et al., 2014). Numerous parametric extensions have been proposed to the Budyko equation (e.g. Choudhury, 1999; Fu, 1981, etc.) and a general solution has been mathematically derived that captures the catchment characteristics in a single parameter (H. Yang et al., 2008). The relationship described by Budyko also emerges from process-based hydrological models (e.g. R. J. Donohue et al., 2012; Entekhabi & Rodriguez-Iturbe, 1994; Feng et al., 2015; Porporato et al., 2004, etc.).

Early approaches for estimating subsurface storage deficits, calculated by taking the difference between precipitation and evaporation over time, date back to at least the 1960s (Grindley, 1960, 1968). In the literature, these methods were used mostly to estimate groundwater recharge (e.g. Finch, 2001; Rushton & Ward, 1979; Rushton et al., 2006, etc.) and were limited by spatial and temporal data resolution. More recently, remotely sensed water fluxes have been used to estimate root-zone storage capacities (S_R) at large scales. For example, continental-scale S_R has been estimated using mass balance approaches (e.g. de Boer-Euser et al., 2016; Gao et al., 2014; Stocker et al., 2023) and a methodology for estimating S_R at a global scale has been proposed by Wang-Erlandsson et al. (2016), and extended to account for snow cover by Dralle et al. (2021), which has been used to investigate ecosystem resilience (Singh et al., 2022), plant water-use sensitivity resulting from interannual rainfall variability (Dralle et al., 2020), and drought coping mechanisms in rainforest-savanna transects (Singh et al., 2020). Existing field-scale measurements (e.g. Rempe & Dietrich, 2018), which cannot be extrapolated over larger scales due to the spatial heterogeneity of plant rooting structures across different climates soil types and bedrock weathering patterns (Gentine et al., 2012; Sivandran & Bras, 2013), align well with satellite-derived S_R (McCormick et al., 2021). Root-zone storage capacities calculated via the deficit method influence the proportion of precipitation that returns to the atmosphere, for a given aridity index, in Australian catchments (Cheng et al., 2022). When combined with existing soil water storage capacity datasets (e.g. Gridded National Soil Survey Geography Database (gNATSGO); Soil Survey Staff, 2019), satellite-derived S_R has been used to estimate $S_{bedrock}$ for the contiguous United States (McCormick et al., 2021).

In this study, we examine the extent to which the bedrock root-zone, which extends beneath the typically thin (< 1 m) soil profile, influences water and energy budgets in the western US. More specifically, we investigate how plant access to bedrock water controls water partitioning and latent heat fluxes. We use a simple water balance approach combined with a national soil coverage database (i.e. gNATSGO), gridded water flux data, and a recent dataset of gridded subsurface water storage capacity to provide insights regarding the transfer of water found exclusively in bedrock to the atmosphere. We quantify the total amount of annual evapotranspiration accessed from the bedrock root-zone, and show that plant growth in many parts of the western US relies on bedrock water surprisingly early into the growing season, counter to conventional understandings that bedrock is used only late in the dry season. Finally, we use a random forest model to corroborate the mass-balance inferences of yearly evapotranspiration that is attributed to access to bedrock water reserves.

In providing a simple, reproducible framework for quantifying the impacts of $S_{bedrock}$ on hydrologic and energy partitioning we look to answer three questions: (1) How early into the growing season do plants in asynchronous climates rely on $S_{bedrock}$ to sustain summer growth?; (2) How does access to bedrock water impact the partitioning of precipitation into evapotranspiration versus streamflow?; and (3) What is the latent heat flux associated with plant use of bedrock water?

2 Methods

To assess bedrock controls on water and energy partitioning, we apply two approaches: (1) an annual water balance, which calculates the total inferred yearly evapotranspiration sourced from bedrock by tracking incoming and outgoing water fluxes; and (2) a random forest model, which estimates the total yearly evapotranspiration sourced from bedrock using a selection of input variables considered to be predictors of evapotranspiration. The water balance method provides conservative, lower-bound constraints on bedrock water use based on conservation of mass, while the random forest model represents a 'best estimate' approach that relies on additional climate predictors beyond evapotranspiration and precipitation fluxes.

In both cases, gridded timeseries of water flux data, in combination with an existing soil water capacity dataset (gNATSGO), are used to estimate the mean annual evapotranspiration sourced from bedrock. However, the input variables of the models differ. The water balance method tracks incoming (precipitation) and outgoing (evapotranspiration) fluxes, at a pixel scale, to determine the amount of evapotranspiration that can be attributed to bedrock (i.e. ET in excess of soil water storage) in a typical water year. The random forest approach trains a model that predicts the mean annual evapotranspiration based on a set of variables describing climate and total observed subsurface storage capacity, then replaces the total observed subsurface storage capacity with mapped soil water storage capacity to predict what total mean annual evapotranspiration would be without access to bedrock water storage; the difference in mean annual ET predictions between the model trained on the total storage vs. soil-storage capacity only is used to infer the amount of evapotranspiration attributed to bedrock water storage.

Using the water balance approach, we additionally explore which areas in the western contiguous US are prone to periods when the subsurface deficit is unable to be replenished on an annual basis (Fig. 2). Using these areas, we re-purpose the original random forest model, replacing the average annual root-zone storage deficit (S_R) with maximum root-zone storage deficit (S_{max}), to make inferences about the water partitioning properties of regions where the deficit does not always reset annually. Finally, we investigate the timing of bedrock water use in the growing season and calculate the latent heat energy used to explore the role of plant use of bedrock water on land surface energy fluxes.

2.1 Study Area

We restricted our study area to winter-wet, summer-dry climate regions of the western contiguous US. To identify these climate regions, we use the asynchronicity index (ASI, (Feng et al., 2019)) calculated from monthly TerraClimate precipitation and po-

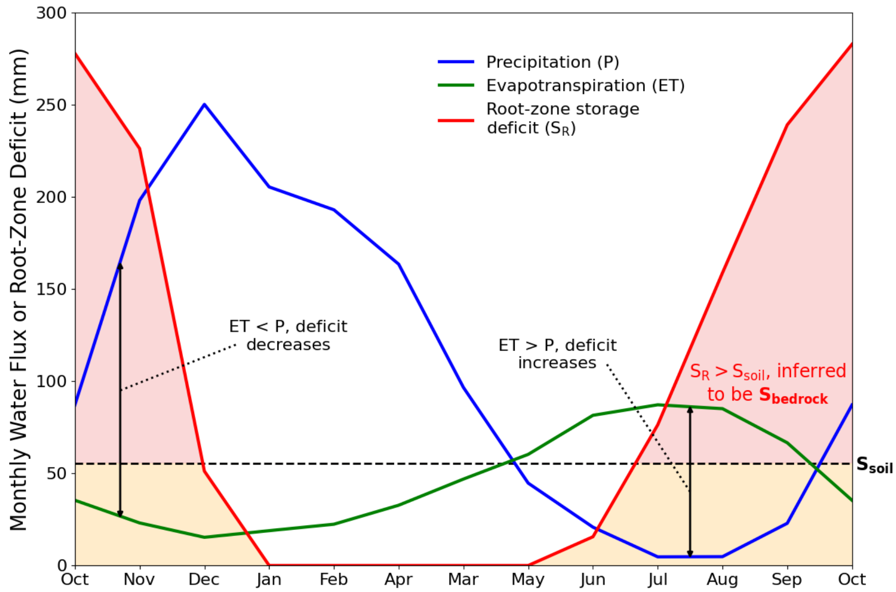

Figure 1. Conceptual diagram describing the root-zone storage characteristics of a typical water year (Oct. 1 - Sep. 30) in regions characterized by asynchronous climates. At the beginning of the wet season, the deficit accrued during the dry season begins to decrease as P > ET. Prior to the beginning of the following dry season, the deficit returns to zero and remains at, or near, zero until ET > P. When ET remains > P such that the deficit surpasses the soil water storage capacity (S_{soil}), plant transpiration is inferred to be a result of access to water stored below the soil layer, i.e. $S_{bedrock}$. Figure is adapted from Lapides et al. (2022b) Fig. 1d.

tential evapotranspiration values (Abatzoglou et al., 2018). We limited the study domain to pixels with an asynchronicity index greater than or equal to 0.40, which is a slightly stricter threshold (0.36) than proposed by (Feng et al., 2019) to designate Mediterranean climates. The masked coverage of the contiguous US, as well as computed asynchronicity index values, are shown in Fig. S1.

We additionally masked out pixels where:

1. long-term evapotranspiration exceeds precipitation, e.g. due to irrigated agricultural lands or data error;
2. land cover is classified as urban or water body; or
3. soil water storage datasets (i.e. gNATSGO) do not have spatial coverage.

For this process, we use a gridded climate product from point observations (Parameter-elevation Regressions on Independent Slopes Model (PRISM); C. Daly et al., 2015), the Penman-Monteith-Leuning ET product (Y. Zhang et al., 2019), the United States Geological Survey (USGS) National Land Cover Database (NLCD) land cover classification (L. Yang et al., 2018), and the Gridded National Soil Survey Geographic Database (Soil Survey Staff, 2019). The pixel masking process follows the methodology defined by McCormick et al. (2021).

All gridded timeseries data, including the products described above, are taken for the 2003 to 2017 water years (Oct. 1 - Sep. 30) and analyzed with the Google Earth Engine Python application programming interface (API) (Gorelick et al., 2017).

2.2 Evaluating Storage via Water Balances

Following McCormick et al. (2021), we estimate a lower-bound on the maximum annual root-zone storage deficit (S_R) using the mass balance approached outlined by Wang-Erlandsson et al. (2016) and expanded to account for snow cover by Dralle et al. (2021) (500 m pixel scale). The technique takes the running integrated difference of land-atmosphere water fluxes exiting (F_{out} [L/T] = ET) and entering (F_{in} [L/T] = P) at a pixel. ET is sourced from PML V2 (500 m pixel scale; Y. Zhang et al., 2019) to represent F_{out} and P is extracted from PRISM (4638.3 m pixel scale; C. Daly et al., 2015), to represent F_{in}. Input data was converted from native resolution (shown in parentheses above) to 1000 m and re-projected to the World Geodetic System 1984 (EPGS:4326) for analysis.

First, the accumulated difference between F_{out} and F_{in} is taken for timeframe t_n to t_{n+1} and corrected for the presence of snow based on a snow cover threshold:

$$A_{t_n \to t_{n+1}} = \int_{t_n}^{t_{n+1}} (1 - \lceil C - C_0 \rceil) \cdot F_{out} - F_{in} \mathrm{d}t \tag{1}$$

where C_0 is a pre-defined threshold percentage of snow cover, C is snow cover, and $\lceil \cdot \rceil$ is the ceiling operator. When $C > C_0$, F_{out} is unaltered; when $C \leq C_0$, F_{out} is set to 0, thereby ignoring ET when snowmelt may be present. This effectively avoids erroneously accumulating a storage deficit from ET during snowmelt when water may be infiltrating into the root zone (without the need to run a full snowmelt model). We use the Normalized Difference Snow Index (NDSI) snow cover band (Hall et al., 2016) to compute snow cover and set the snow cover threshold to 10%.

Second, the instantaneous root-zone storage deficit can be determined iteratively via the following equation:

$$D_{t_{n+1}} = \max(0, D_{t_n} + A_{t_n \to t_{n+1}}) \tag{2}$$

where $D_{t_{n+1}}$ is the deficit at time t_{n+1}. If the deficit falls below zero, the cumulative volume resets to zero as the subsurface has been replenished with water.

At each pixel, we compute the mean annual maximum deficit (D_{max}, evaluated Oct. 1 $\to$ Sep. 30) and infer it to be a lower-bound on annual root-zone storage capacity (S_R). Crucially, this assumes the root-zone storage deficit is replenished on a year-to-year basis which, in many parts of western US, has been shown to not be the case (e.g. Fig. 2; Cui et al., 2022; Goulden & Bales, 2019; Hahm et al., 2022). We then calculate the maximum root-zone storage capacity over the entire study period without the assumption of annual replenishment (S_{max}, evaluated Oct. 1 2002 $\to$ Sep. 30 2017) to investigate multi-year deficit accrual using the random forest model outlined in Sec. 2.5. We use Eq. 2 to calculate D over the entire study period and take the maximum of those values to represent the lower-bound maximum root-zone storage capacity between Oct. 1 2002 (start) and Sep. 30 2017 (end):

$$\underset{t_{start} \to t_{end}}{S_{max}} = \max(D_{t_{start}}, D_{t_{start+1}}, \ldots, D_{t_{end}}) \tag{3}$$

$ET_{bedrock}$, the minimum annual amount of evapotranspiration sourced from bedrock water storage, is inferred to be the difference between the average maximum annual root-zone storage deficit and the soil water storage capacity reported by the Gridded National Soil Survey Geographic Database (Soil Survey Staff, 2019). If the mean annual maximum root-zone storage deficit does not exceed the reported value by gNATGSO, we take this to mean that $S_{bedrock}$ is not needed to explain annual evapotranspiration and set $S_{bedrock} = 0$. This does not necessarily mean that bedrock water storage was not used to support evapotranspiration, but rather that the deficit tracking approach is unable to detect it.

Finally, we compute the average first month of year ($MOY_{bedrock}$) when bedrock must be used to explain observed evapotranspiration, by determining the observed month (for the 2003 - 2017 water years) when mean annual root-zone deficit exceeds the total amount of available storage in the soil, implying any evapotranspiration sourced from the subsurface beyond this date must include water sourced from bedrock storage. This does not mean that bedrock storage was not accessed in prior months but rather that it cannot be tracked using the deficit approach. Therefore, this is the latest possible month that bedrock water is used, because it assumes that i) ET is first sourced from S_{soil} until it is completely depleted, and ii) that deficits are replenished annually, which may not be the case.

2.3 Water Partitioning

Within the Budyko (1974) framework, the long-term partitioning of P into ET and Q is a function of the long-term ratio of PET to P. Under these conditions, Q is assumed to include both overland runoff and lateral subsurface flow resulting from infiltration (hence $\Delta S \approx 0$). We took observed evaporative indices ($\epsilon_{obs} = ET/P$) by dividing the mean annual evapotranspiration by precipitation for the 2003 - 2017 water years using data collected from the gridded products described above. We also infer what the evaporative index would be if plants did not have access to bedrock water ($\epsilon_{w/o\ bedrock}$) by removing $S_{bedrock} = S_R - S_{soil}$ (the minimum amount of bedrock water used in an average year) from the observed evaporative index. If S_R does not exceed S_{soil}, then our method cannot detect the influence of bedrock on the evaporative index:

$$\epsilon_{w/o\ bedrock} = \begin{cases} ET_{obs}\ /\ P & \text{if } S_R \leq S_{soil} \\ [ET_{obs} - (S_R - S_{soil})]\ /\ P & \text{if } S_R > S_{soil} \end{cases} \tag{4}$$

Following this, the relative change (expressed as a percentage) in evaporative index without access to bedrock water is the difference between $\epsilon_{w/o\ bedrock}$ and ϵ_{obs} relative to ϵ_{obs}:

$$\Delta\epsilon = \left(\frac{\epsilon_{w/o\ bedrock} - \epsilon_{obs}}{\epsilon_{obs}}\right) * 100 \tag{5}$$

Streamflow data from 128 minimally impacted USGS watershed gauges in the western US are in agreement (Nash-Sutcliffe efficiency of 0.93) with the precipitation (PRISM) and evapotranspiration (PML) data used in our analysis (Fig. S2). Therefore, we find it reasonable to estimate Q from the water balance (i.e. Q = P - ET) as, over long time frames, the net groundwater flow out of a catchment is negligible (i.e. $\Delta S \approx 0$). We calculated the runoff ratio (RR) as the difference between one and the observed evaporative index ($RR = 1 - \epsilon$).

2.4 Energy Partitioning

We infer the monthly total latent heat flux associated with evapotranspiration sourced from bedrock. The latent heat, i.e. the energy required to change from the liquid to vapor phase, is equal to the the energy required to evaporate the accrued monthly deficit (in mm of water) beyond that provided by soil. We report this value in units of power per unit of area (W/m^2). First, we take the total bedrock water storage extracted for evapotranspiration between two months:

$$ET_{bedrock,\ month} = max(0,\ min(D_{i+1} - D_i,\ D_{i+1} - S_{soil})) \tag{6}$$

where D_i is the deficit at the beginning of month i. To account for the deficit sourced from S_{soil}, the difference between months i and i+1 is compared against the difference between month i+1 and S_{soil}, returning the lesser of the two values. If this value is below zero, bedrock was not needed to account for evapotranspiration during the month and $ET_{bedrock,\,month}$ is set to zero. This calculation assumes that plants first exhaust any available soil water and subsequently use bedrock water. If plants exhaust soil water and bedrock water simultaneously throughout the dry season, the method used here to quantify the total latent heat flux associated with bedrock water during the dry season is not erroneous but rather would shift the bedrock-associated latent heat flux patterns earlier into the dry season.

Secondly, $ET_{bedrock,\,month}$ (mm) is converted to power per unit area metric (E_e) based on the enthalpy of vaporization of a known mass of water:

$$E_e = (ET_{bedrock,\,month}) * (\rho_w) * (\Delta H_v) * (1/t) \tag{7}$$

where ρ_w is the density of water (1000 g/L), ΔH_v is the latent heat of vaporization of water (2257 J/g), which we do not adjust for local variations in temperature or pressure, and t is the total seconds between the ith and i+1th month (1 mm of liquid water per square meter is one liter). The resulting value is an average latent heat flux per second (i.e. power, W) per m^2 (unit area) for a given time frame.

2.5 Random Forest Model

The random forest regression model represents an alternative approach to calculating $ET_{bedrock}$, and is employed here as a means of corroborating the lower-bound, water mass balance inferences described above. The approach uses climatic (ASI and Φ) and subsurface storage (S_R) characteristics to train a model to predict observed mean annual evapotranspiration, and then feeds S_{soil} in place of S_R into the trained model to determine what mean annual ET would be without access to bedrock water storage.

Random forest regression is a predictive machine learning algorithm that consists of a collection of decision trees, which are randomly populated with samples, where the final output is the average of the results of each individual tree (Breiman, 2001). Each individual model (tree) is uncorrelated, producing many unrelated errors which, when combined into a single collective model, will increase prediction accuracy. We use three input variables: S_R, ASI, and Φ to predict annual evapotranspiration. All random forest regression models were implemented using the Random Forest module provided by Scikit-learn, an open-source Python machine learning package (Pedregosa et al., 2011). The random forest model was trained by randomly selecting 70% of the data as a training set and setting 30% aside for validation purposes. Hyperparameters were set to default (scikit-learn v1.3.0) with the exception of minimum leaf samples and maximum features, which were set to 5 (default is 1) and the square root of the number of features (1.0), respectively. Hyperparameters were chosen to best optimize computing time as tweaking the hyperparameters did not significantly improve model performance. The model was run using 20, 40, 80, 120, and 200 trees with improvements in the models performance beyond 40 trees being negligible. Therefore, we chose to run the final product using 40 trees to minimize computing time.

ASI values are calculated using the method outlined by Feng et al. (2019). Following Eq. 2, S_R values can be quantified by taking the mean of the maximum deficit observed each water year, resetting the deficit annually. Φ is measured by taking annual cumulative PET (ΣPET) relative to P (ΣP) and averaging across all water years. P and PET are summed monthly totals taken from TerraClimate (Abatzoglou et al., 2018). We then replace S_R with S_{soil} and re-run the analysis using the predictive model produced using S_R. Framed another way, we forced the model to assume there is no longer access to $S_{bedrock}$ to infer changes in annual evapotranspiration without access to bedrock reserves.

Table 1. Description of referenced variables

Variable	Dimensions	Description
A	L	Accumulated difference; calculated as F_{out} - F_{in} over a given timeframe
ASI	(-)	Asynchronicity index
C	(-)	Snow cover
C_0	(-)	Snow cover threshold
D_{max}	L	Maximum observed annual root-zone deficit
D_{min}	L	Minimum observed root-zone storage deficit in a year
$D_{t_{n+1}}$	L	Root-zone storage deficit measured at time t_{n+1}
E_e	MT^{-3}	Latent heat flux associated with evapotranspiration sourced from bedrock water storage, expressed as power per unit area
ET	LT^{-1}	Evapotranspiration
ET_{obs}	LT^{-1}	Observed evapotranspiration
$ET_{bedrock}$	LT^{-1}	Minimum annual evapotranspiration sourced from bedrock water storage
$ET_{bedrock,\,month}$	L	Monthly (dry season) evapotranspiration sourced from bedrock water storage
F_{in}	LT^{-1}	Inflow
F_{out}	LT^{-1}	Outflow
$MOY_{bedrock}$	(-)	Average month of year when bedrock is needed to explain evapotranspiration
n	(-)	Variable used to quantify differences in the evaporative index for a particular aridity index, defined by (H. Yang et al., 2008)
P	LT^{-1}	Precipitation
P_{obs}	LT^{-1}	Observed precipitation
PET	LT^{-1}	Potential evapotranspiration
Q	LT^{-1}	Runoff (streamflow)
RR	(-)	Runoff ratio; calculated as $1-\epsilon$
$S_{bedrock}$	L	Minimum plant-available water storage capacity in bedrock, inferred from largest deficit in an average water year less mapped S_{soil}
S_{max}	L	The minimum root-zone plant-available storage capacity, inferred from maximum deficit observed over entire time period of analysis
S_R	L	Mean annual root-zone storage capacity inferred from maximum deficit observed over a water year
S_{soil}	L	The maximum amount of plant-available water capable of being stored in the soil profile, from soils mapping
t	T	Time
ΔH_v	ML^{2}T^{-2}	Enthalpy of vaporization of water
ΔS	LT^{-1}	Change in storage
$\Delta\epsilon$	(-)	Relative difference between ϵ_{obs} and $\epsilon_{w/o\,bedrock}$
ϵ	(-)	Evaporative index; calculated as ET/P
ϵ_{obs}	(-)	Observed evaporative index; calculated as ET_{obs}/P_{obs}
$\epsilon_{w/o\,bedrock}$	(-)	Observed evaporative index without bedrock water storage; calculated as ϵ_{obs} $(ET_{obs} - S_{bedrock}/P_{obs})$
ρ_w	L^{-3}M	Density of water
Φ	(-)	Aridity index; calculated as PET/P

Finally, following the extended methodology of Sec. 2.2, which removes the assumption of a yearly resetting deficit, we isolate pixels that have observed multi-year deficit accruals during the study period to investigate the influence of extended drought conditions on water partitioning. Between Oct. 1 2002 and Sep. 30 2017, we calculate the number of years where the deficit was not replenished by taking the minimum root-zone storage deficit (D_{min}) observed each water year for all pixels. If $D_{min} > 0$ in a given water year, we take that to mean that the deficit was not replenished in that water year. The resulting pixels were divided into three classes: 1) Deficit resets annually (all years), 2) Deficit resets most years (deficit resets >66% of the years), and 3) Deficit resets intermittently (deficit resets <66% of the years) (Fig. 2). For these pixels, we amend the original random forest model to use S_{max}, as opposed to S_R, in order to better represent the extent to which $S_{bedrock}$ alters hydrologic partitioning in areas where multi-year deficits occur. All other model characteristics (i.e. hyperparameters, input variables, etc.) were retained from the original random forest model.

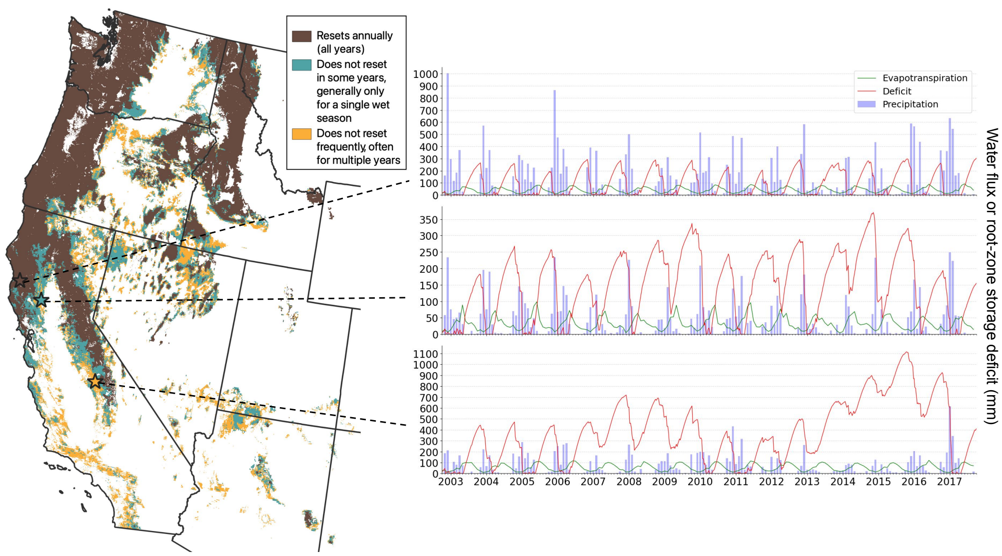

Figure 2. During the study period (Oct. 1 2002 to Sep. 30 2017), the annual deficit returned to zero every year for the regions shown in brown (map on the left). Regions shown in teal and orange, respectively, did not reset in some years (<33% of the study period) or did not reset frequently, often for multiple years in a row (>33%). For each category, a corresponding example time series of the study period is shown on the right with the relevant fluxes necessary to compute root-zone storage deficit. In forests covering over 26,500 km^2 (land covers 1-5 in Fig. S21), the root-zone storage deficit does not reset annually.

3 Results

Our primary findings are that i) soil water storage capacity (S_{soil}) does not explain deviations from the Budyko-curve in asynchronous climates (Fig. 3), ii) the proportion of terrestrial precipitation returned to the atmosphere (vs. streamflow) is strongly influenced by plant use of bedrock water reserves (Fig. 4), iii) $S_{bedrock}$ is needed to sustain dry season plant transpiration surprisingly early into the growing season (Fig. 5), and iv) the summer latent heat flux associated with evapotranspiration of bedrock water is substantial (Fig. 7) and warrants further research with respect to land surface energy interactions. Below, we expand on these findings and highlight particular regions of interest where $S_{bedrock}$ plays an important role in the local water and energy partitioning patterns.

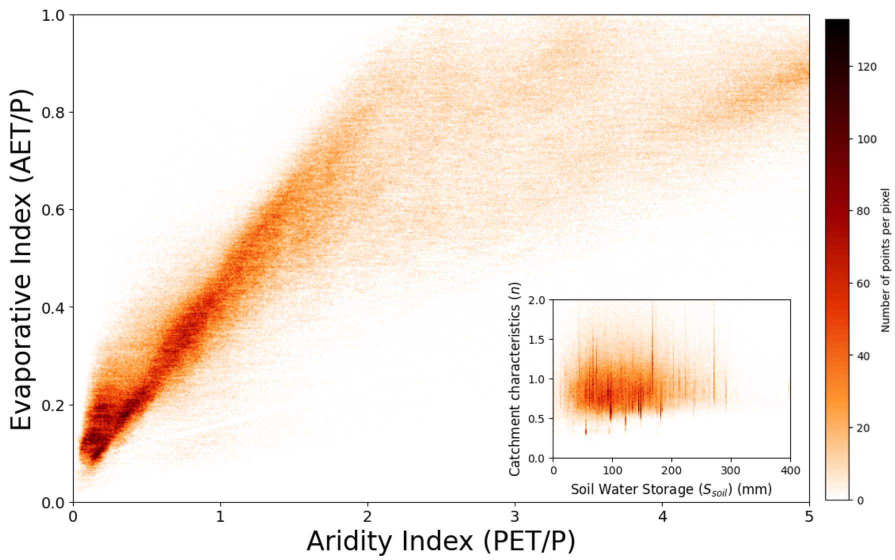

Figure 3. More water is returned to the atmosphere for a given precipitation (higher evaporative index) in locations with more potential evapotranspiration relative to precipitation (aridity index), as shown in this Budyko-space density plot of individual pixels (1000m) with asynchronous climates ($ASI \geq 0.40$) in contiguous United States. The evaporative index for a particular aridity index (expressed in terms of the catchment characteristic, n, where higher n denotes a higher evaporative index for a particular aridity index, see (H. Yang et al., 2008) for derivation) is not well explained by soil water storage (S_{soil}), as shown by the density plot inset.

3.1 Deviations From the Budyko-curve are Poorly Explained by Soil Water Storage Capacity

In our asynchronous climate ($ASI \geq 0.40$) study area, the aridity index explains the primary trend in the evaporative index for individual pixels, consistent with the Budyko (1974) findings for catchments (Fig. 3). However, for a given aridity index, there remain deviations from the curve. It is a commonly hypothesized that, for a particular climate (held constant here by the use of ASI), subsurface storage capacity may explain deviations from the Budyko-curve (Miller et al., 2012). Using the catchment characteristic n to quantify differences in the evaporative index for a particular aridity index (H. Yang et al., 2008), where higher n denotes higher ET/P for a given aridity index, we find that soil water storage capacity (S_{soil}) alone only explains 11% ($R^2 = 0.11$) of the variance in n and, therefore, is a poor explanation for deviations from the Budyko-curve across western US (Fig. 3 inset). Indeed, S_{soil} accounts for only a portion of the below-ground storage capacity and, in many places, is comparatively small relative to $S_{bedrock}$ (e.g. Mc-Cormick et al., 2021). Removing ET sourced from bedrock ($ET_{bedrock}$) drastically shifts the Budyko-curve (Fig. S4). In the following sections, we explore the extent to which $S_{bedrock}$ may control water and energy partitioning.

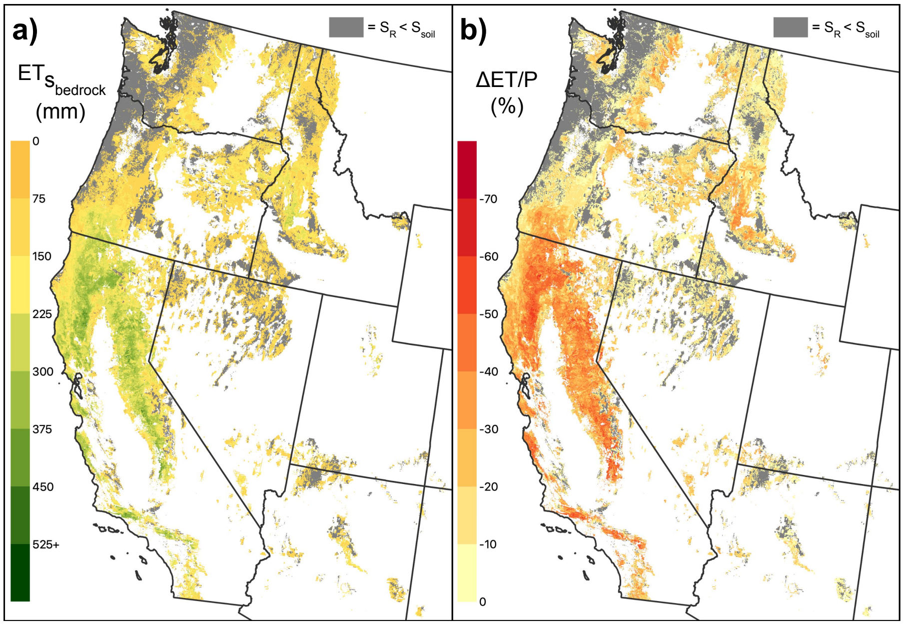

Figure 4. (a) Average value of the largest annually (water year) observed root-zone storage deficit (S_R) in excess of S_{soil}. (b) The relative change in evaporative index when evapotranspiration inferred to be sourced from bedrock storage ($ET_{bedrock}$) is removed, i.e. $(ET - ET_{S_{bedrock}})/P$. (a) inspired by Fig. 3 of McCormick et al. (2021). Across large areas of the western US, annual evapotranspiration would be hundreds of millimeters less and the proportion of precipitation returned to the atmosphere would decrease without access to bedrock water.

3.2 Large Proportions of the Precipitation Returned to the Atmosphere is Sourced from $S_{bedrock}$

In the following section, the spatial patterns of $ET_{bedrock}$, ET/P, and Q/P in the western US, derived using the water balance and random forest methods, are presented. Fig. 4 shows the spatial patterns of evapotranspiration inferred to be sourced from bedrock ($ET_{bedrock}$) and relative change in evaporative index without access to bedrock ($\Delta ET/P$) using the water balance method (see Fig. S5 and S6 for derivation). The corresponding figures using the random forest model can be found in the supplementary information Figs. S9 (ET), S10 (ET/P), and S11 (Q/P). In each case, areas shown in gray represent pixels where bedrock-derived ET was unable to be identified by the proposed methods.

Across the western US, the evaporative index is up to 91% higher (favoring ET) as a result of plant access to bedrock water reserves as opposed to using soil water storage alone. Broadly, evapotranspiration inferred to be sourced from bedrock ($ET_{bedrock}$) increases and relative evaporative index decreases moving south from the USA-Canada border (Fig. 4). In particular, the Northern California Coast Ranges, the southern Cascades, the Transverse Ranges and the Sierra Nevada are most reliant on $S_{bedrock}$ for dry season transpiration. The mean and median changes in relative evaporative index of all pixels in the western US that detected $S_{bedrock}$ use were -16.6 and -13.2%, respectively, using the water balance method. Up to 782 mm of evapotranspiration is inferred to be sourced from bedrock water with mean and median values of 75.8 and 47.9 mm across all pixels, respectively. Areas highlighted in gray did not detect evapotranspiration sourced from bedrock using the deficit approach (i.e. $S_R < S_{soil}$). These areas are mostly limited to the coastal Pacific Northwest, where the aridity index tends to be lower than the rest of the region (Fig. S3), and account for roughly one quarter of all pixels in the study.

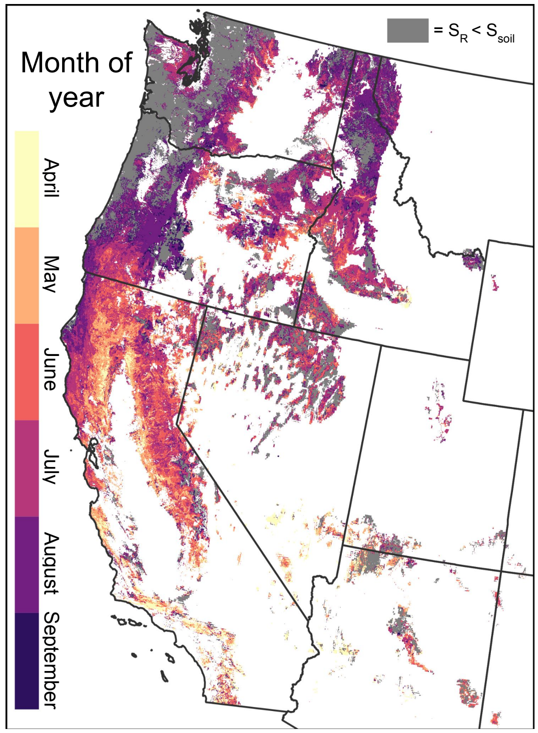

Figure 5. Typical month in which the annual root-zone storage deficit (S_R) exceeds the soil water storage capacity (S_{soil}), implying plant transpiration beyond this point must be using $S_{bedrock}$ to sustain growth. Patterns suggest bedrock water is needed to sustain plant growth very early into the growing season for many parts of the western US.

The random forest model driven by mean annual maximum observed $S_{bedrock}$ makes qualitatively similar predictions ($R^2 = 0.965$; Fig. S8) to the water balance approach based on mean yearly values (Fig. 6). Areas with a non-resetting deficit are more reliant on $S_{bedrock}$ to sustain mean annual evapotranspiration when S_{max} is substituted for S_R. In these areas, S_{max} exceeds S_R by a median value of 82.4 mm (Fig. S20) and S_{soil} values are low (Fig. S5). For transparency the original model informed by S_R was re-run in non-resetting pixels as well (Figs. S12-S15). Using only non-resetting pixels (i.e. teal and orange in Fig. 2), predicted mean and median $ET_{bedrock}$ increased from 87.1 and 54.4 mm to 100.1 and 70.4 mm, respectively, when S_R was substituted with S_{max} and a new random forest model was run (Fig. S17). Similarly, mean (median) relative evaporative index ($\epsilon_{w/o\, bedrock}$) decreased from -19.0% (-14.8) to -23.5% (-22.6) when accounting for a non-resetting deficit (Fig. S18-S19). Interestingly, when S_{max} is used as an predictor instead of S_R, the relative importance of aridity index as a predictor increases substantially (Fig. S16).

3.3 $S_{bedrock}$ is Needed to Sustain Plant Growth Early into the Growing Season and Contributes Substantial Latent Heat Flux as Summer Progresses

Regions of high $ET_{bedrock}$ (Fig. 4, S9) also correspond to areas that require $S_{bedrock}$ to sustain plant growth surprisingly early into the growing season (Fig. 5) and involve large bedrock-water associated latent heat fluxes in the hot summer months (Fig. 7). The average first day of the year when $S_{bedrock}$ is needed to account for evapotranspiration (in other words when $S_R > S_{soil}$) is 190 (July 9) and over 21% of the study area must use bedrock water to account for ET prior to the beginning of summer (June 21) (Fig.

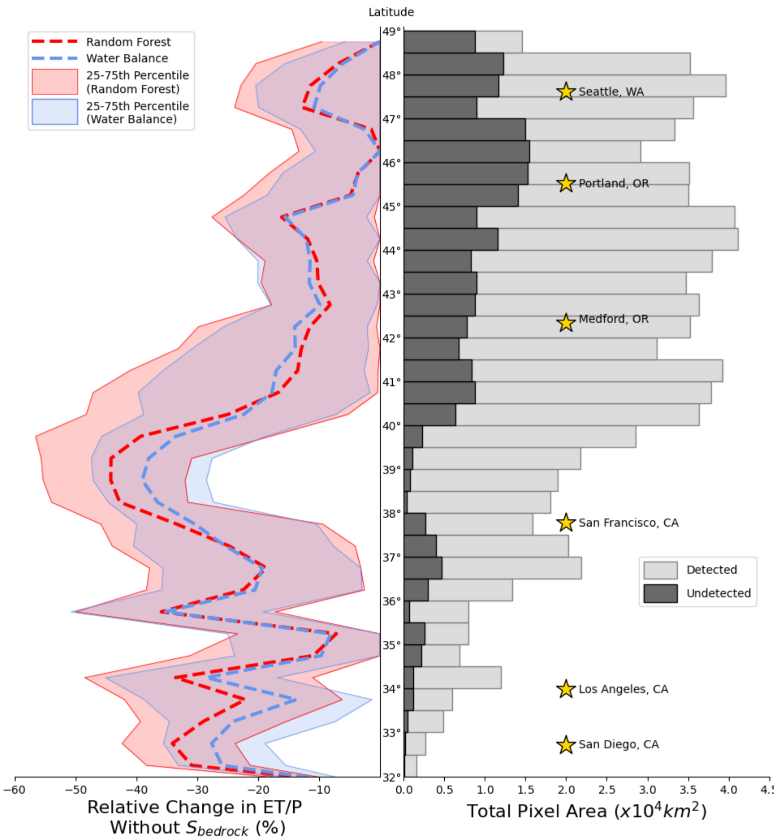

Figure 6. On the left, binned (0.5°) relative change in evaporative index (ET/P) without access to $S_{bedrock}$ using the water balance method (blue) and random forest model (red). On the right, the total area of pixels within each latitudinal band (gray) and the total area of pixels where ET sourced from bedrock water ($ET_{bedrock}$) was not detected using the water balance method (black). Stars show to the latitudinal locations of relevant major cities in the western United States. Across all latitudes, the random forest model predictions align closely with the results of the annual water balance model.

S7). In June, the majority of the study area in California has a noticeable latent heat flux associated with ET sourced from bedrock. By August, there is widespread latent heat flux across the western US, with July and August having the highest average values.

4 Discussion

The findings presented in this study highlight the importance of $S_{bedrock}$ on water and energy partitioning in the western US. Below we discuss the possible implications of these findings on land-atmosphere interactions. We begin by situating our study within the context of the Budyko framework and discuss how this influences hydrologic partitioning. We then discuss the role of factors like geology on controlling the amount of $S_{bedrock}$ and, consequently, hydrologic and energy partitioning. Finally, we address limitations to our study and offer potential future opportunities to advance the topic.

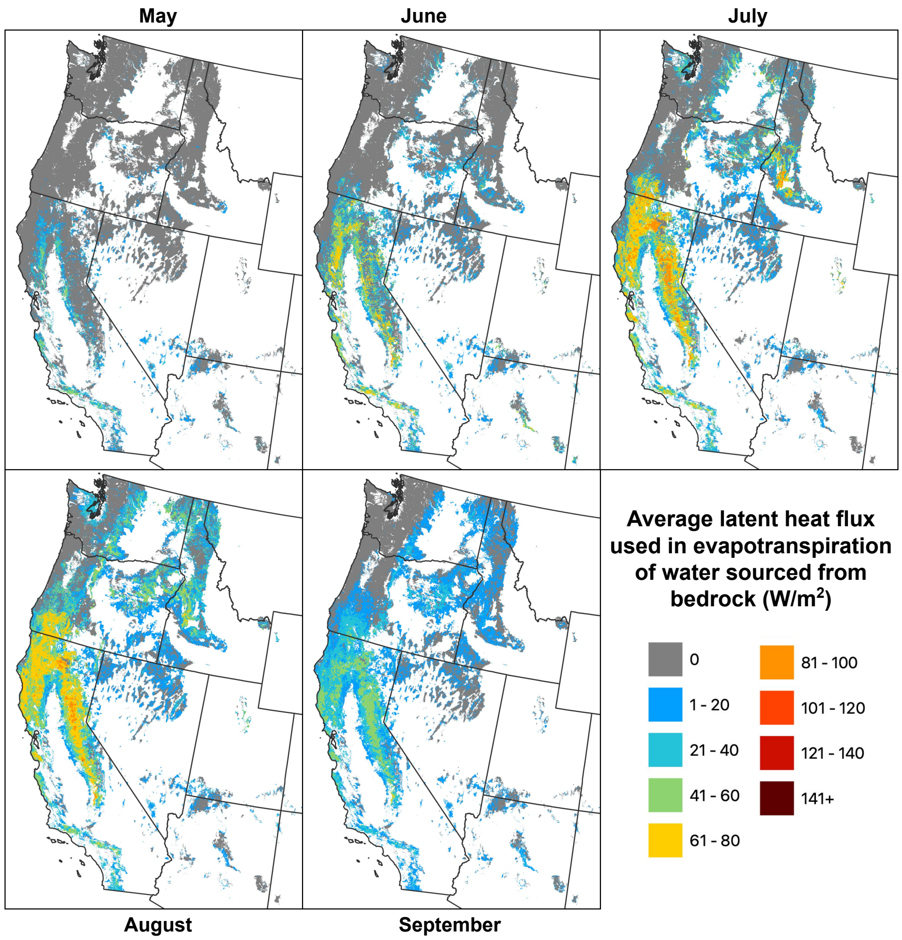

Figure 7. Average latent heat flux (equivalent units to solar irradiance, W/m^2) used in evapotranspiration that is sourced from $S_{bedrock}$ during the growing season. In large parts of the western US, in particular northern California and the Sierra Nevada mountain ranges, a large latent heat flux is associated with evapotranspiration of bedrock water every summer.

4.1 $S_{bedrock}$ Controls on Water and Energy Partitioning

The catchment water balance in asynchronous climates often deviates substantially from expectations set by the Budyko curve (Berghuijs et al., 2020; De Lavenne & Andréassian, 2018; Potter et al., 2005; Viola et al., 2017). We found that in the western US, asynchronicity and root-zone storage capacity are two of the strongest predictors for mean annual evapotranspiration (Figs S8, S12, S16), consistent with previous studies focusing on soil water storage that showed that ET is favored with increasing soil water storage capacity (Feng et al., 2012; Milly, 1994a, 1994b; Padrón et al., 2017; Porporato et al., 2004), as well as studies highlighting the importance of seasonality (Feng et al., 2012; Gerrits et al., 2009; Hickel & Zhang, 2006; Xing et al., 2018; Yokoo et al., 2008) and water storage capacity (Chen et al., 2013; Cheng et al., 2022; E. Daly et al., 2019; R. J. Donohue et al., 2012; Gentine et al., 2012; Hickel & Zhang, 2006; Milly, 1994a, 1994b; Potter et al., 2005; Rodriguez-Iturbe et al., 1999; Williams et al., 2012; Woods, 2003). We take this analysis a step further, by differentiating soil from bedrock, to elucidate basic features of how root-zone water is divided between hydrogeologically distinct subsurface layers. Our results suggest S_{soil} alone poorly explains deviations from the Budyko-curve

(Fig. 3), and indicate that $S_{bedrock}$ plays a comparatively larger role on controlling hydrologic partitioning in the western US. This is confirmed by our findings in Figs. 4, S4-S6, S9-11, and is in agreement with similar findings by McCormick et al. (2021), and hillslope-scale observational studies (Dralle et al., 2018; Hahm et al., 2019b, 2022; Lapides et al., 2022a; Rempe & Dietrich, 2018). Moreover, if $S_{bedrock}$ influences near-surface climate properties in a similar manner to soil moisture (e.g. Brabson et al., 2005; Koster et al., 2004; Haarsma et al., 2009), current GCMs may under-estimate the influence of subsurface storage on extreme temperatures and heat waves (e.g. Seneviratne et al., 2006; Diffenbaugh et al., 2007), precipitation formation (e.g. Alfieri et al., 2008; Ek & Holtslag, 2004; Taylor, 2015), and changes in planetary boundary layer (PBL) circulation patterns (e.g. Sousa et al., 2020; Ookouchi et al., 1984).

4.2 $S_{bedrock}$ Influences on Runoff Generation

Some forms of runoff generation require unsaturated storage deficits to be replenished prior to significant runoff production (McDonnell et al., 2021; Sayama et al., 2011). Recently, Lapides et al. (2022b) showed that the 'missing' snowmelt runoff during the 2021 spring melt period in California (California Department of Water Resources, 2021) could be attributed to deep root-zone storage deficits caused by drought conditions. These areas, and many other parts of the western US, have among the largest observed S_R in the contiguous US and the fraction of S_R attributed to bedrock is substantial (McCormick et al., 2021). Our results agree with these findings and highlight that $S_{bedrock}$ has major implications for runoff generation in the mountainous West. Deficit-based approaches represent a potential method for scaling up hillslope (e.g. S. P. Anderson et al., 1997; Salve et al., 2012; Tromp-van Meerveld et al., 2007), catchment (e.g. Ajami et al., 2011), and watershed-scale (e.g. Sayama et al., 2011) studies to explain and predict runoff production—the "Holy Grail" of hydrology (Beven, 2006)—at large scales. While our findings suggest bedrock storage heavily influences runoff patterns, especially in southwest (Fig. S11), there is a need for more studies investigating these dynamics and, in particular, field-scale studies to confirm the trends presented here.

4.3 Geological Influences on $S_{bedrock}$ as a Controlling Factor in Vegetation Structure

Evidence supporting the notion that forest ecosystems rely on moisture stored in weathered bedrock to sustain dry season growth goes back several decades (e.g. Arkley, 1981; Jones & Graham, 1993; Rose et al., 2003; Witty et al., 2003). In many cases, bedrock water constitutes a majority of the total subsurface water available to sustain transpiration (e.g. M. Anderson et al., 1995; Hubbert, Graham, & Anderson, 2001; Rose et al., 2003; McCormick et al., 2021). Here, we demonstrate that bedrock storage dynamics influence water and energy partitioning at large scales and throughout many parts of the western US. The extent of bedrock weathering impacts its pore size distribution with depth, and therefore plant-available water storage properties (Klos et al., 2018; Dawson et al., 2020). These properties in turn depend on climate, tectonics, and geology. The mechanisms responsible for the transformation of fresh to weathered bedrock, which in turn increases subsurface moisture storage potential, are well established (see for overview, e.g. S. L. Brantley, 2010; Graham et al., 2010) but remain difficult to investigate due to limitations in accessing deep bedrock samples (see for overview, e.g. Zanner & Graham, 2005). Recently, the Critical Zone (CZ) sciences community has proposed methods for predicting weathered bedrock patterns (Riebe et al., 2017) based on advancements in geophysics (e.g. Slim et al., 2015; St. Clair et al., 2015), geochemistry (e.g. S. Brantley et al., 2013; Lebedeva et al., 2007; Lebedeva & Brantley, 2013), and geomorphology (e.g. R. S. Anderson et al., 2013; Rempe & Dietrich, 2014). A reliable and testable method for predicting weathered bedrock patterns would serve as an important stepping stone in understanding the complex interactions between subsurface properties and aboveground processes. For example, root-zone storage capacities and plant community composition have been shown to differ drastically in two adjacent, climatically similar watersheds in California due to contrasting geological substrates (Hahm et al., 2019b). More recently, Hahm et al. (2023) highlighted areas where geologic substrates overlapped with lower than 'climatically expected' S_R and argued that plant growth in these areas is inhibited directly by porosity and/or permeability (e.g. Hahm et al., 2019b; Jiang et al., 2020; H. Liu et al., 2021) or indirectly via nutrient limitation (e.g. Hahm et al., 2014) and toxicity (e.g. Kruckeberg, 1992). However, extending these findings to include the influence of bedrock structure and geology on hydrologic partitioning has not been investigated. The present study underscores the necessity to further investigate bedrock weathering mechanisms as we move towards a holistic approach in CZ sciences.

5 Limitations

Limiting our study to distributed, remotely sensed, or spatially interpolated datasets may introduce substantial uncertainty in the results. Although the prevalence of systematic errors (e.g. cloud filtering, sensors, etc.) is a known limitation to using remotely sensed data, we found that precipitation (PRISM) in excess of evapotranspiration (PML) aligned well with USGS streamflow data in 128 minimally impacted catchments in our study area (Fig. S2 and Rempe et al. (2022)). There are limited field data to validate our inferences; however, McCormick et al. (2021) synthesised existing datasets and found the observations that were consistent with deficit-based methods. The accuracy of satellite-based data has improved dramatically in recent decades (Dubovik et al., 2021) and, when coupled with finer-scale field studies (i.e. watershed to hillslope), allows for macro-scale assimilation of topics that underpin important hydrologic problems. While we are confident in the data presented here we emphasize the need to further implement field-based studies.

To calculate the annual water balance, we first explored the scenario in which the subsurface storage deficit returned to zero annually. This is not always the case. There is ample evidence suggesting that many western forests have prolonged, multi-year deficits (e.g. Cui et al., 2022; Goulden & Bales, 2019; Hahm et al., 2022; P.-W. Liu et al., 2022). During our analysis we calculated the number of instances per pixel where the subsurface storage deficit did not return to zero in a given year and concluded that, in many cases, the deficit either resets intermittently or very infrequently. When isolating for areas where the deficit has been shown to not reset, our findings suggest that $S_{bedrock}$ plays an even bigger role in hydrologic and energy partitioning than previously suggested by our annual water balance and corroborative random forest model. Despite being limited by some of the lowest soil water storage capacities in the contiguous US (see McCormick et al. (2021) Extended Data Fig. 2b), these areas boast many of the largest maximum root-zone storage (S_{max}) values computed between 2003 - 2017 and, consequently, the largest $S_{bedrock}$. The importance of $S_{bedrock}$ to dry season plant transpiration in asynchronous climates is not a new idea (e.g. McCormick et al., 2021; Milly, 1994a); however, research underpinned by these ideas rarely accounts for the possibility of multi-year deficits. We posit that $S_{bedrock}$ is likely underestimated in areas with non-resetting deficits and that, in regions that are currently transitioning towards Mediterranean climates as a result of warming trends (e.g. British Columbia), the magnitude of available $S_{bedrock}$ may be a limiting factor of future plant growth. In the results section, we reported the typical day (and month) of year when evapotranspiration begins using $S_{bedrock}$ based on the proposed water balance model and argued that $S_{bedrock}$ is necessary to sustain growth early into the dry season for many parts of the western US. We did not recalculate this value using a multi-year deficit for regions where the deficit does not return to zero annually. However, assuming wet season precipitation fully percolates into $S_{bedrock}$ prior to the dry season, we expect many areas are permanently using $S_{bedrock}$ to sustain summer growth.

6 Conclusion

In this study, we introduce a simple and reproducible annual water balance framework for assessing the role of $S_{bedrock}$ on water partitioning within the context of the Budyko framework. We employ this framework to investigate the timing of evapotranspiration inferred to be sourced from $S_{bedrock}$ and the magnitude of summer latent heat flux produced as a result of access to $S_{bedrock}$. Finally, we use a random forest regression algorithm to corroborate our findings and then re-purpose the random forest model to explore further areas where the root-zone storage deficit does not reset annually. Our findings suggest that, in the western contiguous US: 1) $S_{bedrock}$ is necessary to explain plant transpiration very early into the growing season; 2) the proportion of precipitation returning to atmosphere would drastically decrease without access to $S_{bedrock}$; 3) the amount of latent heat flux produced as a result evapotranspiration sourced from bedrock is substantial during the summer; and 4) in regions where the root-zone storage deficit frequently does not reset, the magnitude of evapotranspiration sourced from $S_{bedrock}$ is greater, thereby further influencing the water and energy partitioning properties. These results confirm that $S_{bedrock}$ plays a key role in the local hydrologic cycle and potentially influences the severity and frequency of wildfire and mass die-off events. Further research contributing to the role of $S_{bedrock}$ on the land surface energy balance — e.g. extreme temperatures, heat waves, wind patterns, etc. — would prove beneficial in understanding the factors governing tree death and wildfire, an issue that is prevalent across the western US.

7 Open Research

Flux data (ET, P, PET, and Q) were obtained from Penman-Monteith-Leuning Evapotranspiration (L. Zhang et al., 2001), Parameter-elevation Regressions on Independent Slopes Model (`https://prism.oregonstate.edu`), TerraClimate (`https://www.climatologylab.org/terraclimate.html`), and Catchment Attributes and Meteorology for Large-sample Studies (`https://ral.ucar.edu/solutions/products/camels`), respectively. Land cover, soil water storage, and snow cover were obtained from USGS National Land Cover Database (`https://www.mrlc.gov/data`), Gridded National Soil Survey Geographic Database (`https://www.nrcs.usda.gov/resources/data-and-reports/gridded-national-soil-survey-geographic-database-gnatsgo#download`), and the National Snow and Ice Data Center (`https://nsidc.org/data/mod10a1/versions/61`). All data products were analyzed using the Google Earth Engine Python API (Gorelick et al., 2017). Data, figures, and code associated with this manuscript are available publicly at the following repository on Hydroshare: (Ehlert et al., 2023; Bedrock controls on water and energy partitioning across the western contiguous United States, HydroShare, `https://doi.org/10.4211/hs.191353753cc44de891ee392b95aae22b`).

Acknowledgments

Funding was provided by Simon Fraser University, a Natural Sciences and Engineering Research Council of Canada Discovery grant, and Canadian Foundation for Innovation/British Columbia Knowledge Development Fund held by W. J. Hahm.

References

Abatzoglou, J. T., Dobrowski, S. Z., Parks, S. A., & Hegewisch, K. C. (2018). Terraclimate, a high-resolution global dataset of monthly climate and climatic water balance from 1958–2015. *Scientific data*, *5*(1), 1–12.

Ajami, H., Troch, P. A., Maddock III, T., Meixner, T., & Eastoe, C. (2011). Quantifying mountain block recharge by means of catchment-scale storage-discharge relationships. *Water Resources Research*, *47*(4).

Alfieri, L., Claps, P., D'Odorico, P., Laio, F., & Over, T. M. (2008). An analysis of the soil moisture feedback on convective and stratiform precipitation. *Journal of Hydrometeorology*, *9*(2), 280–291.

Anderson, M., Graham, R., Alyanakian, G., & Martynn, D. (1995). Late summer water status of soils and weathered bedrock in a giant sequoia grove. *Soil Science*, *160*(6), 415–422.

Anderson, R. S., Anderson, S. P., & Tucker, G. E. (2013). Rock damage and regolith transport by frost: An example of climate modulation of the geomorphology of the critical zone. *Earth Surface Processes and Landforms*, *38*(3), 299–316.

Anderson, S. P., Dietrich, W. E., Montgomery, D. R., Torres, R., Conrad, M. E., & Loague, K. (1997). Subsurface flow paths in a steep, unchanneled catchment. *Water Resources Research*, *33*(12), 2637–2653.

Arkley, R. J. (1981). Soil moisture use by mixed conifer forest in a summer-dry climate. *Soil Science Society of America Journal*, *45*(2), 423–427.

Berghuijs, W. R., Gnann, S. J., & Woods, R. A. (2020). Unanswered questions on the budyko framework. *Journal of Hydrology*, *265*, 164–177.

Beven, K. (2006). Searching for the holy grail of scientific hydrology: Q t=(s, r, δt) a as closure. *Hydrology and earth system sciences*, *10*(5), 609–618.

Brabson, B., Lister, D., Jones, P., & Palutikof, J. (2005). Soil moisture and predicted spells of extreme temperatures in britain. *Journal of Geophysical Research: Atmospheres*, *110*(D5).

Brantley, S., Lebedeva, M., & Bazilevskaya, E. (2013). Relating weathering fronts for acid neutralization and oxidation to pco2 and po2. In *The atmosphere-history* (pp. 327–352). Elsevier Inc.

Brantley, S. L. (2010). Rock to regolith. *Nature Geoscience*, *3*(5), 305–306.

Breiman, L. (2001). Random forests. *Machine learning*, *45*, 5–32.

Budyko, M. I. (1974). *Climate and life*. Academic press.

California Department of Water Resources, C. (2021, September). Water year 2021: An extreme year. Retrieved 2021-09-30, from `https://water.ca.gov/-/media/DWR-Website/Web-Pages/Water-Basics/Drought/Files/Publications-And-Reports/091521-Water-Year-2021-broch_v2.pdf`

Chen, X., Alimohammadi, N., & Wang, D. (2013). Modeling interannual variability of seasonal evaporation and storage change based on the extended budyko framework. *Water Resources Research*, *49*(9), 6067–6078.

Cheng, S., Cheng, L., Qin, S., Zhang, L., Liu, P., Liu, L., ... Wang, Q. (2022). Improved understanding of how catchment properties control hydrological partitioning through machine learning. *Water Resources Research*, *58*(4), e2021WR031412.

Choudhury, B. (1999). Evaluation of an empirical equation for annual evaporation using field observations and results from a biophysical model. *Journal of Hydrology*, *216*(1-2), 99–110.

Cui, G., Ma, Q., & Bales, R. (2022). Assessing multi-year-drought vulnerability in dense mediterranean-climate forests using water-balance-based indicators. *Journal of Hydrology*, *606*, 127431.

Daly, C., Smith, J. I., & Olson, K. V. (2015). Mapping atmospheric moisture climatologies across the conterminous united states. *PloS one*, *10*(10), e0141140.

Daly, E., Calabrese, S., Yin, J., & Porporato, A. (2019). Hydrological spaces of long-term catchment water balance. *Water Resources Research*, *55*(12), 10747–10764.

Dawson, T. E., Hahm, W. J., & Crutchfield-Peters, K. (2020). Digging deeper: what the critical zone perspective adds to the study of plant ecophysiology. *New Phytologist*, *226*(3), 666–671.

de Boer-Euser, T., McMillan, H. K., Hrachowitz, M., Winsemius, H. C., & Savenije, H. H. (2016). Influence of soil and climate on root zone storage capacity. *Water Resources Research*, *52*(3), 2009–2024.

De Lavenne, A., & Andréassian, V. (2018). Impact of climate seasonality on catchment yield: A parameterization for commonly-used water balance formulas. *Journal of Hydrology*, *558*, 266–274.

Diffenbaugh, N. S., Pal, J. S., Giorgi, F., & Gao, X. (2007). Heat stress intensification in the mediterranean climate change hotspot. *Geophysical Research Letters*, *34*(11).

Donohue, R., Roderick, M., & McVicar, T. R. (2007). On the importance of including vegetation dynamics in budyko's hydrological model. *Hydrology and Earth System Sciences*, *11*(2), 983–995.

Donohue, R. J., Roderick, M. L., & McVicar, T. R. (2012). Roots, storms and soil pores: Incorporating key ecohydrological processes into budyko's hydrological model. *Journal of Hydrology*, *436*, 35–50.

Dralle, D. N., Hahm, W. J., Chadwick, K. D., McCormick, E., & Rempe, D. M. (2021). Accounting for snow in the estimation of root zone water storage capacity from precipitation and evapotranspiration fluxes. *Hydrology and Earth System Sciences*, *25*(5), 2861–2867.

Dralle, D. N., Hahm, W. J., Rempe, D. M., Karst, N., Anderegg, L. D., Thompson, S. E., … Dietrich, W. E. (2020). Plants as sensors: vegetation response to rainfall predicts root-zone water storage capacity in mediterranean-type climates. *Environmental Research Letters*, *15*(10), 104074.

Dralle, D. N., Hahm, W. J., Rempe, D. M., Karst, N. J., Thompson, S. E., & Dietrich, W. E. (2018). Quantification of the seasonal hillslope water storage that does not drive streamflow. *Hydrological processes*, *32*(13), 1978–1992.

Dubovik, O., Schuster, G. L., Xu, F., Hu, Y., Bösch, H., Landgraf, J., & Li, Z. (2021). *Grand challenges in satellite remote sensing* (Vol. 2). Frontiers Media SA.

Durre, I., Wallace, J. M., & Lettenmaier, D. P. (2000). Dependence of extreme daily maximum temperatures on antecedent soil moisture in the contiguous united states during summer. *Journal of climate*, *13*(14), 2641–2651.

Ek, M., & Holtslag, A. (2004). Influence of soil moisture on boundary layer cloud development. *Journal of hydrometeorology*, *5*(1), 86–99.

Entekhabi, D., & Rodriguez-Iturbe, I. (1994). Analytical framework for the characterization of the space-time variability of soil moisture. *Advances in water resources*, *17*(1-2), 35–45.

Feng, X., Porporato, A., & Rodriguez-Iturbe, I. (2015). Stochastic soil water balance under seasonal climates. *Proceedings of the Royal Society A: Mathematical, Physical and Engineering Sciences*, *471*(2174), 20140623.

Feng, X., Thompson, S. E., Woods, R., & Porporato, A. (2019). Quantifying asynchronicity of precipitation and potential evapotranspiration in mediterranean climates. *Geophysical Research Letters*, *46*(24), 14692–14701.

Feng, X., Vico, G., & Porporato, A. (2012). On the effects of seasonality on soil water balance and plant growth. *Water resources research*, *48*(5).

Finch, J. (2001). Estimating change in direct groundwater recharge using a spatially distributed soil water balance model. *Quarterly Journal of Engineering Geology and Hydrogeology*, *34*(1), 71–83.

Fischer, E. M., Seneviratne, S. I., Vidale, P. L., Lüthi, D., & Schär, C. (2007). Soil moisture–atmosphere interactions during the 2003 european summer heat wave. *Journal of Climate*, *20*(20), 5081–5099.

Fu, B. (1981). On the calculation of the evaporation from land surface. *Scientia Atmospherica Sinica*, *5*(1), 23.

Gao, H., Hrachowitz, M., Schymanski, S., Fenicia, F., Sriwongsitanon, N., & Savenije, H. (2014). Climate controls how ecosystems size the root zone storage capacity at catchment scale. *Geophysical Research Letters*, *41*(22), 7916–7923.

Gentine, P., D'Odorico, P., Lintner, B. R., Sivandran, G., & Salvucci, G. (2012).

Interdependence of climate, soil, and vegetation as constrained by the budyko curve. *Geophysical Research Letters*, *39*(19).
Gerrits, A., Savenije, H., Veling, E., & Pfister, L. (2009). Analytical derivation of the budyko curve based on rainfall characteristics and a simple evaporation model. *Water Resources Research*, *45*(4).
Gorelick, N., Hancher, M., Dixon, M., Ilyushchenko, S., Thau, D., & Moore, R. (2017). Google earth engine: Planetary-scale geospatial analysis for everyone. *Remote sensing of Environment*, *202*, 18–27.
Goulden, M. L., & Bales, R. C. (2019). California forest die-off linked to multi-year deep soil drying in 2012–2015 drought. *Nature Geoscience*, *12*(8), 632–637.
Graham, R., Rossi, A., & Hubbert, R. (2010). Rock to regolith conversion: Producing hospitable substrates for terrestrial ecosystems. *GSA today*, *20*, 4–9.
Grindley, J. (1960). Calculated soil moisture deficits in the dry summer of 1959 and forecast dates of first appreciable runoff. *International Association of Scientific Hydrology*, 109–120.
Grindley, J. (1968). The estimation of soil moisture deficits. *Water for Peace: Water Supply Technology*, *3*, 241.
Haarsma, R. J., Selten, F., Hurk, B. v., Hazeleger, W., & Wang, X. (2009). Drier mediterranean soils due to greenhouse warming bring easterly winds over summertime central europe. *Geophysical research letters*, *36*(4).
Hahm, W. J., Dralle, D. N., Lapides, D. A., Ehlert, R. S., & Rempe, D. (2023). Geologic controls on apparent root-zone storage capacity. *Authorea Preprints*.
Hahm, W. J., Dralle, D. N., Sanders, M., Bryk, A. B., Fauria, K. E., Huang, M.-H., . . . others (2022). Bedrock vadose zone storage dynamics under extreme drought: consequences for plant water availability, recharge, and runoff. *Water Resources Research*, *58*(4), e2021WR031781.
Hahm, W. J., Rempe, D., Dralle, D., Dawson, T., & Dietrich, W. (2020). Oak transpiration drawn from the weathered bedrock vadose zone in the summer dry season. *Water Resources Research*, *56*(11), e2020WR027419.
Hahm, W. J., Rempe, D. M., Dralle, D. N., Dawson, T. E., Lovill, S. M., Bryk, A. B., . . . Dietrich, W. E. (2019b). Lithologically controlled subsurface critical zone thickness and water storage capacity determine regional plant community composition. *Water Resources Research*, *55*(4), 3028–3055.
Hahm, W. J., Riebe, C. S., Lukens, C. E., & Araki, S. (2014). Bedrock composition regulates mountain ecosystems and landscape evolution. *Proceedings of the National Academy of Sciences*, *111*(9), 3338–3343.
Hall, D., Riggs, G., & Salomonson, V. (2016). Modis/terra snow cover daily l3 global 500m grid, version 6. *Boulder, CO: NASA National Snow and Ice Data Center Distributed Active Archive Center*.
Hickel, K., & Zhang, L. (2006). Estimating the impact of rainfall seasonality on mean annual water balance using a top-down approach. *Journal of Hydrology*, *331*(3-4), 409–424.
Hubbert, K., Beyers, J., & Graham, R. (2001). Roles of weathered bedrock and soil in seasonal water relations of pinus jeffreyi and arctostaphylos patula. *Canadian Journal of Forest Research*, *31*(11), 1947–1957.
Hubbert, K., Graham, R., & Anderson, M. (2001). Soil and weathered bedrock: components of a jeffrey pine plantation substrate. *Soil Science Society of America Journal*, *65*(4), 1255–1262.
Jasechko, S., Sharp, Z. D., Gibson, J. J., Birks, S. J., Yi, Y., & Fawcett, P. J. (2013). Terrestrial water fluxes dominated by transpiration. *Nature*, *496*(7445), 347–350.
Jensen, D., Reager, J. T., Zajic, B., Rousseau, N., Rodell, M., & Hinkley, E. (2018). The sensitivity of us wildfire occurrence to pre-season soil moisture conditions across ecosystems. *Environmental research letters*, *13*(1), 014021.
Jiang, Z., Liu, H., Wang, H., Peng, J., Meersmans, J., Green, S. M., . . . Song, Z.

(2020). Bedrock geochemistry influences vegetation growth by regulating the regolith water holding capacity. *Nature communications*, *11*(1), 2392.

Jones, D., & Graham, R. (1993). Water-holding characteristics of weathered granitic rock in chaparral and forest ecosystems. *Soil Science Society of America Journal*, *57*(1), 256–261.

Klos, P. Z., Goulden, M. L., Riebe, C. S., Tague, C. L., O'Geen, A. T., Flinchum, B. A., ... others (2018). Subsurface plant-accessible water in mountain ecosystems with a mediterranean climate. *Wiley Interdisciplinary Reviews: Water*, *5*(3), e1277.

Koster, R. D., Dirmeyer, P. A., Guo, Z., Bonan, G., Chan, E., Cox, P., ... others (2004). Regions of strong coupling between soil moisture and precipitation. *Science*, *305*(5687), 1138–1140.

Kruckeberg, A. (1992). Plant life of western north american ultramafics. *The ecology of areas with serpentinized rocks: a world view*, 31–73.

Lapides, D. A., Hahm, W. J., Rempe, D. M., Dietrich, W. E., & Dralle, D. N. (2022a). Controls on stream water age in a saturation overland flow-dominated catchment. *Water Resources Research*, *58*(4), e2021WR031665.

Lapides, D. A., Hahm, W. J., Rempe, D. M., Whiting, J., & Dralle, D. N. (2022b). Causes of missing snowmelt following drought. *Geophysical Research Letters*, *49*(19), e2022GL100505.

Lebedeva, M. I., & Brantley, S. L. (2013). Exploring geochemical controls on weathering and erosion of convex hillslopes: Beyond the empirical regolith production function. *Earth Surface Processes and Landforms*, *38*(15), 1793–1807.

Lebedeva, M. I., Fletcher, R. C., Balashov, V., & Brantley, S. L. (2007). A reactive diffusion model describing transformation of bedrock to saprolite. *Chemical Geology*, *244*(3-4), 624–645.

Lhomme, J.-P., & Moussa, R. (2016). Matching the budyko functions with the complementary evaporation relationship: consequences for the drying power of the air and the priestley–taylor coefficient. *Hydrology and Earth System Sciences*, *20*(12), 4857–4865.

Liu, H., Dai, J., Xu, C., Peng, J., Wu, X., & Wang, H. (2021). Bedrock-associated belowground and aboveground interactions and their implications for vegetation restoration in the karst critical zone of subtropical southwest china. *Progress in Physical Geography: Earth and Environment*, *45*(1), 7–19.

Liu, M., Lin, K., & Cai, X. (2022). Climate and vegetation seasonality play comparable roles in water partitioning within the budyko framework. *Journal of Hydrology*, *605*, 127373.

Liu, P.-W., Famiglietti, J. S., Purdy, A. J., Adams, K. H., McEvoy, A. L., Reager, J. T., ... Rodell, M. (2022). Groundwater depletion in california's central valley accelerates during megadrought. *Nature Communications*, *13*(1), 7825.

McCormick, E. L., Dralle, D. N., Hahm, W. J., Tune, A. K., Schmidt, L. M., Chadwick, K. D., & Rempe, D. M. (2021). Widespread woody plant use of water stored in bedrock. *Nature*, *597*(7875), 225–229.

McDonnell, J. J., Spence, C., Karran, D. J., Van Meerveld, H., & Harman, C. J. (2021). Fill-and-spill: A process description of runoff generation at the scale of the beholder. *Water Resources Research*, *57*(5), e2020WR027514.

Miller, J. D., Collins, B. M., Lutz, J. A., Stephens, S. L., Van Wagtendonk, J. W., & Yasuda, D. A. (2012). Differences in wildfires among ecoregions and land management agencies in the sierra nevada region, california, usa. *Ecosphere*, *3*(9), 1–20.

Milly, P. (1994a). Climate, interseasonal storage of soil water, and the annual water balance. *Advances in Water Resources*, *17*(1-2), 19–24.

Milly, P. (1994b). Climate, soil water storage, and the average annual water balance. *Water Resources Research*, *30*(7), 2143–2156.

Ookouchi, Y., Segal, M., Kessler, R., & Pielke, R. (1984). Evaluation of soil moisture effects on the generation and modification of mesoscale circulations. *Monthly weather review*, *112*(11), 2281–2292.

Padrón, R. S., Gudmundsson, L., Greve, P., & Seneviratne, S. I. (2017). Large-scale controls of the surface water balance over land: Insights from a systematic review and meta-analysis. *Water Resources Research*, *53*(11), 9659–9678.

Pedregosa, F., Varoquaux, G., Gramfort, A., Michel, V., Thirion, B., Grisel, O., … others (2011). Scikit-learn: Machine learning in python. *the Journal of machine Learning research*, *12*, 2825–2830.

Porporato, A., Daly, E., & Rodriguez-Iturbe, I. (2004). Soil water balance and ecosystem response to climate change. *The American Naturalist*, *164*(5), 625–632.

Potter, N., Zhang, L., Milly, P., McMahon, T. A., & Jakeman, A. (2005). Effects of rainfall seasonality and soil moisture capacity on mean annual water balance for australian catchments. *Water Resources Research*, *41*(6).

Rakhmatulina, E., Stephens, S., & Thompson, S. (2021). Soil moisture influences on sierra nevada dead fuel moisture content and fire risks. *Forest Ecology and Management*, *496*, 119379.

Rempe, D. M., & Dietrich, W. E. (2014). A bottom-up control on fresh-bedrock topography under landscapes. *Proceedings of the National Academy of Sciences*, *111*(18), 6576–6581.

Rempe, D. M., & Dietrich, W. E. (2018). Direct observations of rock moisture, a hidden component of the hydrologic cycle. *Proceedings of the National Academy of Sciences*, *115*(11), 2664–2669.

Rempe, D. M., McCormick, E. L., Hahm, W. J., Persad, G. G., Cummins, C., Lapides, D. A., … Dralle, D. N. (2022). Resilience of woody ecosystems to precipitation variability.

Riebe, C. S., Hahm, W. J., & Brantley, S. L. (2017). Controls on deep critical zone architecture: A historical review and four testable hypotheses. *Earth Surface Processes and Landforms*, *42*(1), 128–156.

Rodriguez-Iturbe, I., Porporato, A., Ridolfi, L., Isham, V., & Coxi, D. (1999). Probabilistic modelling of water balance at a point: the role of climate, soil and vegetation. *Proceedings of the Royal Society of London. Series A: Mathematical, Physical and Engineering Sciences*, *455*(1990), 3789–3805.

Rose, K., Graham, R., & Parker, D. (2003). Water source utilization by pinus jeffreyi and arctostaphylos patula on thin soils over bedrock. *Oecologia*, *134*, 46–54.

Rushton, K., Eilers, V., & Carter, R. (2006). Improved soil moisture balance methodology for recharge estimation. *Journal of Hydrology*, *318*(1-4), 379–399.

Rushton, K., & Ward, C. (1979). The estimation of groundwater recharge. *Journal of Hydrology*, *41*(3-4), 345–361.

Salve, R., Rempe, D. M., & Dietrich, W. E. (2012). Rain, rock moisture dynamics, and the rapid response of perched groundwater in weathered, fractured argillite underlying a steep hillslope. *Water Resources Research*, *48*(11).

Sayama, T., McDonnell, J. J., Dhakal, A., & Sullivan, K. (2011). How much water can a watershed store? *Hydrological Processes*, *25*(25), 3899–3908.

Seneviratne, S. I., Lüthi, D., Litschi, M., & Schär, C. (2006). Land–atmosphere coupling and climate change in europe. *Nature*, *443*(7108), 205–209.

Singh, C., van der Ent, R., Wang-Erlandsson, L., & Fetzer, I. (2022). Hydroclimatic adaptation critical to the resilience of tropical forests. *Global Change Biology*, *28*(9), 2930–2939.

Singh, C., Wang-Erlandsson, L., Fetzer, I., Rockström, J., & Van Der Ent, R. (2020). Rootzone storage capacity reveals drought coping strategies along rainforest-savanna transitions. *Environmental Research Letters*, *15*(12), 124021.

Sivandran, G., & Bras, R. L. (2013). Dynamic root distributions in ecohydrological modeling: A case study at walnut gulch experimental watershed. *Water Resources Research*, *49*(6), 3292–3305.
Slim, M., Perron, J. T., Martel, S. J., & Singha, K. (2015). Topographic stress and rock fracture: A two-dimensional numerical model for arbitrary topography and preliminary comparison with borehole observations. *Earth Surface Processes and Landforms*, *40*(4), 512–529.
Soil Survey Staff, S. (2019). *Gridded national soil survey geographic (gnatsgo) database for the conterminous united states.* United States Department of Agriculture, Natural Resources Conservation Service.
Sousa, P. M., Barriopedro, D., García-Herrera, R., Ordóñez, C., Soares, P. M., & Trigo, R. M. (2020). Distinct influences of large-scale circulation and regional feedbacks in two exceptional 2019 european heatwaves. *Communications Earth & Environment*, *1*(1), 48.
St. Clair, J., Moon, S., Holbrook, W., Perron, J., Riebe, C., Martel, S., ... Richter, D. d. (2015). Geophysical imaging reveals topographic stress control of bedrock weathering. *Science*, *350*(6260), 534–538.
Stocker, B. D., Tumber-Dávila, S. J., Konings, A. G., Anderson, M. C., Hain, C., & Jackson, R. B. (2023). Global patterns of water storage in the rooting zones of vegetation. *Nature geoscience*, *16*(3), 250–256.
Taylor, C. M. (2015). Detecting soil moisture impacts on convective initiation in europe. *Geophysical Research Letters*, *42*(11), 4631–4638.
Trenberth, K. E., Smith, L., Qian, T., Dai, A., & Fasullo, J. (2007). Estimates of the global water budget and its annual cycle using observational and model data. *Journal of Hydrometeorology*, *8*(4), 758–769.
Tromp-van Meerveld, H., Peters, N., & McDonnell, J. (2007). Effect of bedrock permeability on subsurface stormflow and the water balance of a trenched hillslope at the panola mountain research watershed, georgia, usa. *Hydrological Processes: An International Journal*, *21*(6), 750–769.
Viola, F., Caracciolo, D., Forestieri, A., Pumo, D., & Noto, L. (2017). Annual runoff assessment in arid and semiarid mediterranean watersheds under the budyko's framework. *Hydrological Processes*, *31*(10), 1876–1888.
Wang-Erlandsson, L., Bastiaanssen, W. G., Gao, H., Jägermeyr, J., Senay, G. B., Van Dijk, A. I., ... Savenije, H. H. (2016). Global root zone storage capacity from satellite-based evaporation. *Hydrology and Earth System Sciences*, *20*(4), 1459–1481.
Williams, C. A., Reichstein, M., Buchmann, N., Baldocchi, D., Beer, C., Schwalm, C., ... others (2012). Climate and vegetation controls on the surface water balance: Synthesis of evapotranspiration measured across a global network of flux towers. *Water Resources Research*, *48*(6).
Witty, J. H., Graham, R. C., Hubbert, K. R., Doolittle, J. A., & Wald, J. A. (2003). Contributions of water supply from the weathered bedrock zone to forest soil quality. *Geoderma*, *114*(3-4), 389–400.
Woods, R. (2003). The relative roles of climate, soil, vegetation and topography in determining seasonal and long-term catchment dynamics. *Advances in Water Resources*, *26*(3), 295–309.
Xing, W., Wang, W., Shao, Q., & Yong, B. (2018). Identification of dominant interactions between climatic seasonality, catchment characteristics and agricultural activities on budyko-type equation parameter estimation. *Journal of Hydrology*, *556*, 585–599.
Yang, H., Qi, J., Xu, X., Yang, D., & Lv, H. (2014). The regional variation in climate elasticity and climate contribution to runoff across china. *Journal of hydrology*, *517*, 607–616.
Yang, H., Yang, D., Lei, Z., & Sun, F. (2008). New analytical derivation of the mean annual water-energy balance equation. *Water resources research*, *44*(3).

Yang, L., Jin, S., Danielson, P., Homer, C., Gass, L., Bender, S. M., ... others (2018). A new generation of the united states national land cover database: Requirements, research priorities, design, and implementation strategies. *ISPRS journal of photogrammetry and remote sensing*, *146*, 108–123.

Yokoo, Y., Sivapalan, M., & Oki, T. (2008). Investigating the roles of climate seasonality and landscape characteristics on mean annual and monthly water balances. *Journal of Hydrology*, *357*(3-4), 255–269.

Zanner, C. W., & Graham, R. C. (2005). Deep regolith: exploring the lower reaches of soil. *Geoderma*, *1*(126), 1–3.

Zhang, L., Dawes, W., & Walker, G. (2001). Response of mean annual evapotranspiration to vegetation changes at catchment scale. *Water resources research*, *37*(3), 701–708.

Zhang, Y., Kong, D., Gan, R., Chiew, F. H., McVicar, T. R., Zhang, Q., & Yang, Y. (2019). Coupled estimation of 500 m and 8-day resolution global evapotranspiration and gross primary production in 2002–2017. *Remote sensing of environment*, *222*, 165–182.